

Benchmarking the Ising Universality Class in $3 \leq d < 4$ dimensions

C. Bonanno^{1*}, A. Cappelli¹, M. Kompaniets^{2,3}, S. Okuda⁴, K. J. Wiese⁵

1 INFN, Sezione di Firenze, Via G. Sansone 1, 50019 Sesto Fiorentino (FI), Italy

2 Saint Petersburg State University, 7/9 Universitetskaya Embankment, St. Petersburg, 199034, Russia

3 Bogoliubov Laboratory of Theoretical Physics, JINR, 6 Joliot-Curie, Dubna, 141980, Russia

4 Department of Physics, Rikkyo University Toshima, Tokyo 171-8501, Japan

5 Laboratoire de Physique de l'École Normale Supérieure, Université PSL, CNRS, Sorbonne Université, Université Paris-Diderot, Sorbonne Paris Cité, 24 rue Lhomond, 75005 Paris, France

*claudio.bonanno@fi.infn.it

October 30, 2022

1 Abstract

2 The Ising critical exponents η , ν and ω are determined up to one-per-thousand relative error in the whole range of dimensions $3 \leq d < 4$, using numerical conformal-
3 bootstrap techniques. A detailed comparison is made with results by the resummed
4 epsilon expansion in varying dimension, the analytic bootstrap, Monte Carlo and non-
5 perturbative renormalization-group methods, finding very good overall agreement.
6 Precise conformal field theory data of scaling dimensions and structure constants are
7 obtained as functions of dimension, improving on earlier findings, and providing bench-
8 marks in $3 \leq d < 4$.
9

10

11 Contents

12	1 Introduction	2
13	2 Conformal bootstrap in non-integer dimension	3
14	2.1 Summary of numerical methods	3
15	2.2 Analysis of conformal dimensions of the three leading fields for $4 > d \geq 3$	5
16	3 Comparison with the epsilon expansion in $4 > d \geq 3$	9
17	3.1 Warm-up analysis of the anomalous dimensions γ_σ	9
18	3.2 Bootstrap data versus resummed perturbative results	13
19	4 Structure constants and scaling dimensions of higher fields	20
20	4.1 Structure constants in $4 > d \geq 3$	21
21	4.2 Higher fields T' and C	24
22	4.3 Subleading fields ϵ'' and C'	26

23	5 Conclusions	28
24	A Orthogonal polynomial regression	29
25	B Example of series resummation	31
26	References	34

27
28

29 1 Introduction

30 Many approaches to critical phenomena obtain results in continuous space dimension, although
31 physically relevant dimensions are integer. Most notable is the perturbative renormalization group
32 in $d = 4 - \epsilon$ dimensions [1–4]. This is not merely a technical issue: quantities as functions of real
33 d can clarify features that are harder to see at discrete values. E.g., one can follow the topology
34 of the renormalization-group (RG) flow as a function of dimension and find instances where the
35 universality class changes at non-integer values. This proved particularly useful for systems with
36 long-range interactions [5–7] or disorder [8–13].

37 The recent very precise numerical conformal bootstrap [14–16] has been formulated in continuous
38 dimension [17, 18], in particular for the Ising model in its whole range $4 > d \geq 2$ [19, 20]. The
39 interest lies in understanding how the strongly interacting Ising conformal field theory connects
40 to a free scalar in $d = 4$ and to the integrable fully-solvable model in $d = 2$ [21, 22]. Analytic
41 bootstrap approaches which use the dimension as a tunable parameter were also developed [23–31].
42 Initially, the non-unitarity of the theory in non-integer dimensions [32] was thought to hamper the
43 numerical methods involving positive quantities. These concerns have been overcome by *de facto*
44 never observing problems for the quantities of interest, as explained later.

45 In this paper, we extend the numerical approach of Ref. [19] using a single correlator, the
46 SDPB [33] routine for determining the unitarity domain, and the Extremal Functional Method [34,
47 35] for solving the bootstrap equations. We obtain improved results for the scaling dimensions in
48 $4 > d \geq 3$ by a denser scanning of the unitary region near the Ising point, i.e., the kink. The latter
49 gets parametrically sharper as d approaches 4, allowing for its better identification.

50 The improved precision allows us to perform a detailed comparison with state-of-the-art epsilon
51 expansion in two regimes: for d close to 4, the series is directly compared to bootstrap data,
52 using the necessary finer scale for the latter; for intermediate values between 4 and 3 (included),
53 the divergent perturbative series is resummed using well-established methods involving the Borel
54 transform [36–39].

55 The analysis is done at the level of the precision of our bootstrap data, which is given by the d -
56 independent value $\text{Err}(\gamma)/\gamma = O(10^{-2}, 10^{-3})$, namely the relative error of the anomalous dimensions
57 γ for the conformal fields $\sigma, \epsilon, \epsilon'$, respectively corresponding to spin, energy and subleading energy,
58 and determining the critical exponents η, ν, ω . As the anomalous dimensions are very small for
59 $d \approx 4$, the precision for the conformal dimensions $\Delta_\sigma, \Delta_\epsilon$ is actually higher in this region, while for
60 $\Delta_{\epsilon'}$ it stays at three digits, as explained later. Some of the structure constants are also found with
61 very high precision.

We compare our data with recent results of the numerical [20] and analytic bootstrap [26–31], Monte Carlo simulations [40–42] and the non-perturbative RG [43,44]. We find that the data by all methods agree very well. This is rather rewarding given the achieved precision. Besides confirming the high quality of conformal-bootstrap results, our analysis provides a reference point for further analytic and numerical methods aiming at exploring critical phenomena in varying dimensions.

The outline of this paper is the following. In Sec. 2 we summarize our bootstrap protocol [19] and present the results for the three main conformal dimensions mentioned above, together with their polynomial fits as a function of dimension and the estimation of errors. In Sec. 3 we briefly recall the properties of the epsilon expansion and resummation techniques. We then compare its predictions with our bootstrap data and the results by other methods, and authors. A detailed analysis of all issues is presented. In Sec. 4, we report the numerical bootstrap data for scaling dimensions of other conformal fields and structure constants, and compare them to the existing epsilon expansion. In the conclusions in Sec. 5 we discuss open questions.

2 Conformal bootstrap in non-integer dimension

The aim of this section is to summarize our procedure for deriving conformal data of scaling dimensions and structure constants, as a function of the space-time dimension $4 > d \geq 2$. We first discuss the conformal dimensions of three main fields $\mathcal{O} = \sigma, \epsilon, \epsilon'$. Our goal is to provide a polynomial description of $\Delta_{\mathcal{O}}$ as a function of $y = 4 - d$, by performing a *best fit* of the data obtained at several values of d ¹. Our results are finally compared to those obtained from the resummed epsilon expansion in Section 3.

2.1 Summary of numerical methods

The conformal dimensions and structure constants of the critical Ising model as a function of d are computed in the setup of Ref. [19], which we shortly summarize for the reader's convenience. We consider a single 4-point correlator $\langle \sigma(x_1)\sigma(x_2)\sigma(x_3)\sigma(x_4) \rangle$, where $\sigma(x)$ is the primary scalar field with lowest dimension, denoted Δ_{σ} . We truncate the functional bootstrap equation to 190 components. The unitarity condition for this equation is determined through the SDPB algorithm [33], leading to a bound in the $(\Delta_{\sigma}, \Delta_{\epsilon})$ plane; next, the Extremal Functional Method (EFM) [34,35] is used to solve the equations on this boundary. We use the generalization of these numerical methods to non-integer dimensions developed in Ref. [19], and detailed in its Appendix A.

Our numerical 1-correlator bootstrap approach has been surpassed by more recent implementations in $d = 3$ [16,45,46], but we find it still convenient for determining the low-lying spectrum with modest computing resources. The complete determination of the conformal data for one value of d requires about 20 hours on 256 cores, corresponding to 5000 core hours. This simple setting allows us to evaluate the spectrum for several dimensions d .

The first crucial step is to locate the Ising critical point in parameter space. To this end, we adopt the twofold strategy of Ref. [19], consisting in searching the kink on the unitarity boundary in the $(\Delta_{\sigma}, \Delta_{\epsilon})$ plane and, at the same time, minimizing the central charge c [15]. This procedure allow us to determine for each value of d an interval of values for $\Delta_{\sigma}, \Delta_{\epsilon}$ and c , that we take as the Ising conformal theory, accompanied by an estimate of the uncertainty.

¹Note that ϵ is the energy field, the next-to-lowest scalar primary field, not to be confused with the deviation from

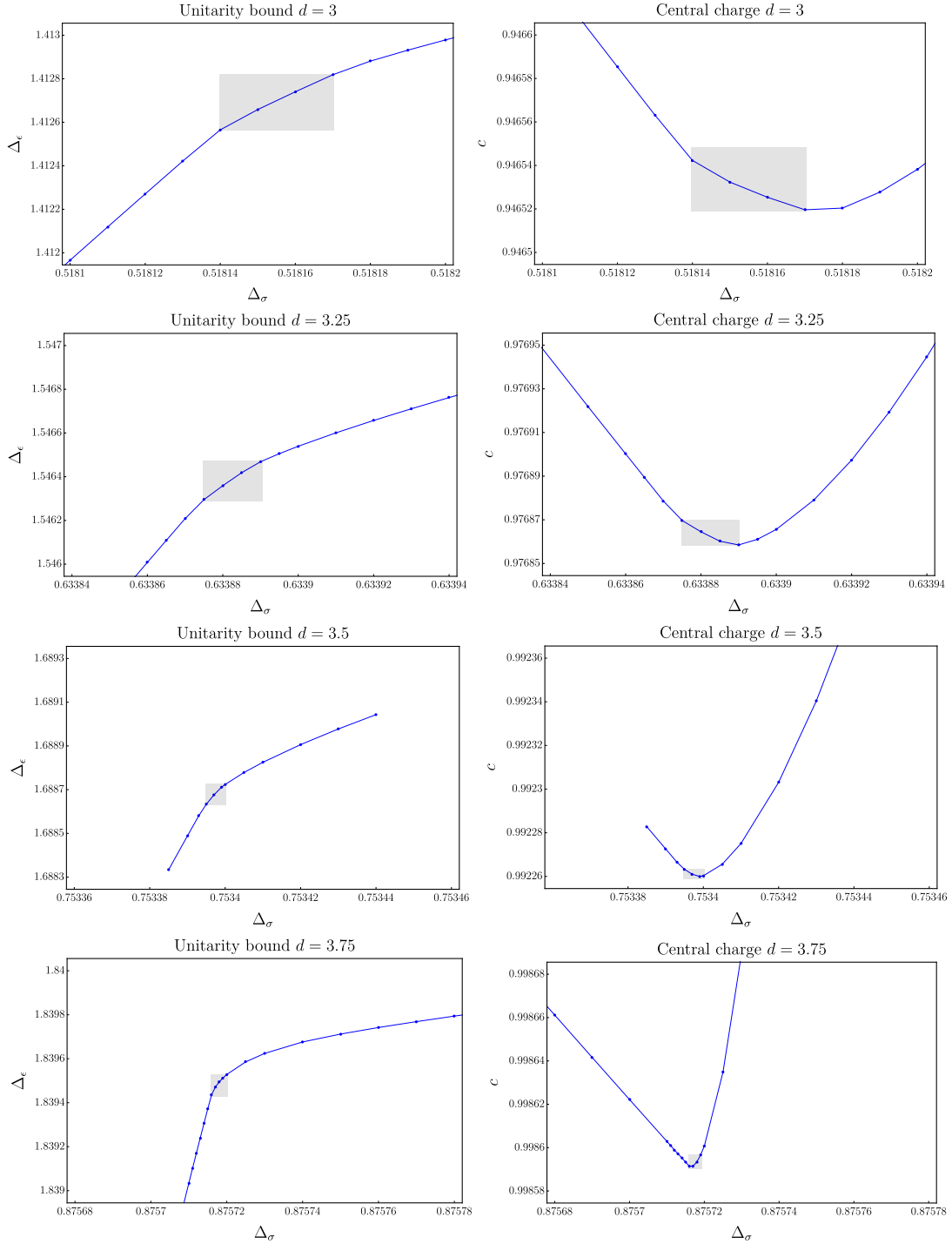


Figure 1: Determination of the Ising critical point for $d = 3, 3.25, 3.5, 3.75$ ($d = 3$ data from Ref. [19]). Left plots: Identification of the kink; the blue points correspond to the solutions of the bootstrap equations. Right plots: position of the c minimum. The grey shaded areas represent the estimated errors on Δ_σ , Δ_ϵ and c .

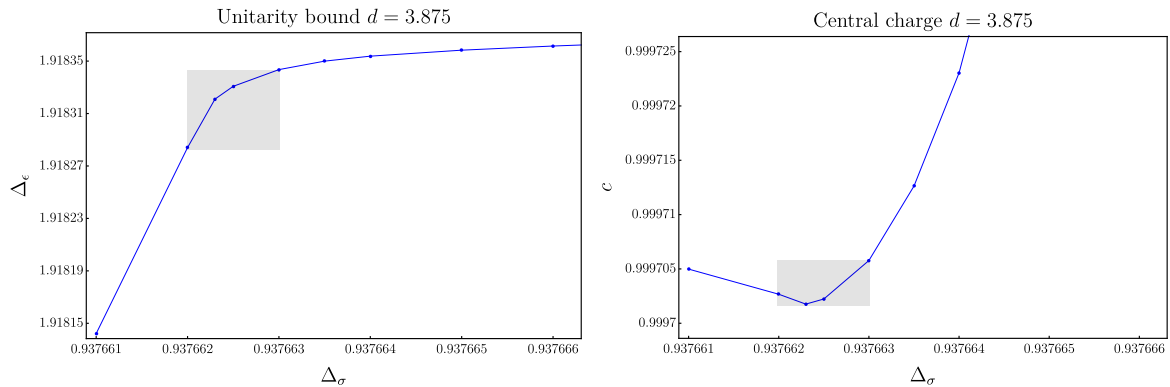


Figure 2: Determination of the Ising point for $d = 3.875$, as in Fig. 1. Note the magnified scale on both axis with respect to those of Fig. 1.

101 This procedure is displayed in Fig. 1, where we show the identification of the Ising point for
 102 $d = 3, 3.25, 3.5$ and 3.75 . The gray area in the plots indicates the chosen errors for $\Delta_\sigma, \Delta_\epsilon$ and
 103 c , which are roughly determined by the mismatch between the positions of the minimum and the
 104 kink. As a conservative choice, we consider an interval of four data points for each value of d .

105 The precision is greater than in Ref. [19], because we perform a finer scan of the Δ_σ values
 106 around the kink. We observe that the kink and the minimum get sharper for $d \rightarrow 4$, as shown by
 107 the four pairs of plots drawn on the same scale in Fig. 1; this is convenient in our approach, since
 108 it leads to an increased precision when anomalous dimensions are smaller. In Fig. 2, we show the
 109 point $d = 3.875$, not considered in the earlier work. It is necessary for studying the region of $d \rightarrow 4$.
 110 Here the curves are so steep that magnified scales are needed.

111 Once the Ising point is determined, we obtain the rest of the conformal data as follows. The
 112 solution of the bootstrap equations gives a spectrum of conformal dimensions $\Delta_{\mathcal{O}}$ and structure
 113 constants $f_{\sigma\sigma\mathcal{O}}$ as a function of Δ_σ ; they are divided into different sets characterized by the spin
 114 $\ell = 0, 2, 4, \dots$ of the operator \mathcal{O} . The estimation of $\Delta_{\mathcal{O}}$ and $f_{\sigma\sigma\mathcal{O}}$ is obtained by taking the central
 115 value of such quantities for Δ_σ varying in the interval previously identified as the Ising point (grey
 116 areas in Figs. 1 and 2). The error is obtained from their dispersion.

117 It is interesting to point out that, although we largely improved the precision of our results for
 118 $4 > d > 3$ with respect to Ref. [19], we observe no signs of trouble associated to non-unitarity in
 119 our bootstrap spectrum. On general grounds, non-unitarity contributions are expected to appear
 120 for non-integer values of d due to the presence of negative-norm states [32]. However, these occur
 121 at very high order in the OPE expansion of the correlator $\langle \sigma\sigma\sigma\sigma \rangle$, thus we may argue that they
 122 have numerically negligible structure constants. As a matter of fact, their presence does not seem
 123 to yield problems in solving the bootstrap equations with our method. This conclusion was also
 124 reached by recent 3-correlator bootstrap studies of the critical $O(N)$ models [18] and the Ising
 125 model [20] in non-integer space dimensions using the *navigator method* [47].

126 2.2 Analysis of conformal dimensions of the three leading fields for $4 > d \geq 3$

127 In Tab. 1 we present our results for the conformal dimensions $\Delta_{\mathcal{O}}$ in $4 > d > 3$ along with those
 128 of Ref. [19] for $3 \geq d > 2$, also employed in the following. Our implementation of the bootstrap

four dimensions denoted by y .

129 determines with high precision the conformal dimensions and structure constants for the first few
 130 low-lying operators with $\ell = 0, 2$ and 4: $\mathcal{O}_{\ell=0} = \sigma, \epsilon, \epsilon', \mathcal{O}_{\ell=2} = T'$ and $\mathcal{O}_{\ell=4} = C$ [19].

d	Δ_σ	Δ_ϵ	$\Delta_{\epsilon'}$	$\Delta_{\epsilon''}$	$\Delta_{T'}$	Δ_C	$\Delta_{C'}$
4	1	2	4	6	6	6	8
3.875	0.9376625(5)	1.91831(3)	3.992(2)	7.0(3)	5.9307(6)	5.8752253(9)	7.903(3)
3.75	0.8757175(15)	1.83948(4)	3.9771(12)	6.8(2)	5.8616(12)	5.75111(13)	7.81(3)
3.5	0.753398(3)	1.68868(5)	3.9296(8)	6.82(7)	5.734(7)	5.5053(5)	7.55(6)
3.25	0.633883(8)	1.54639(9)	3.8776(11)	6.92(6)	5.59(2)	5.264(2)	7.25(10)
3	0.518155(15)	1.41270(15)	3.8305(15)	7.01(5)	5.505(10)	5.026(4)	6.7(2)
2.75	0.40747(4)	1.2887(2)	3.800(2)	7.12(8)	5.445(15)	4.790(5)	6.3(2)
2.5	0.30341(1)	1.17625(15)	3.7970(10)	7.32(2)	5.46(3)	4.574(9)	5.78(13)
2.25	0.20822(3)	1.0784(2)	3.847(1)	7.53(2)	5.58(5)	4.344(14)	5.36(6)
2.2	0.19053(8)	1.0610(5)	3.864(4)	7.64(3)	5.69(4)	4.325(15)	5.29(4)
2.15	0.17333(8)	1.0444(4)	3.891(6)	7.73(3)	5.64(13)	4.28(3)	5.19(1)
2.1	0.15663(8)	1.0286(5)	3.9215(5)	7.82(3)	5.820(10)	4.17(4)	5.12(4)
2.05	0.14048(8)	1.0134(7)	3.9565(5)	7.93(3)	5.9050(10)	4.13(6)	5.065(15)
2.01	0.12803(8)	1.001(2)	3.9900(10)	8.035(5)	5.9815(5)	4.01440(10)	5.0115(15)
2.00001	0.125000(10)	0.99989(14)	4.0002(2)	7.99(10)	6.0006(2)	4.000055(10)	5.00048(8)
2	0.125	1	4	8	6	4	5

Table 1: Conformal dimensions of the first few low-lying states for $4 > d > 2$. Exact values for $d = 2, 4$ are given in bold, results for $3 \geq d > 2$ are taken from Ref. [19].

131 The goal of this section is to determine the behavior of $\Delta_{\mathcal{O}}$ as a function of the variable $y = 4 - d$,
 132 by finding the best fitting polynomial that describes the data in Tab. 1. We use all available values,
 133 but focus on the range of $4 > d \geq 3$ where results are more precise and allow for a comparison with
 134 other approaches. The points for $3 > d \geq 2$ are mainly used for stabilizing the higher powers of
 135 the fitting polynomials².

136 We employ an improved fit method for $\Delta_{\mathcal{O}}(y)$ that uses orthogonal polynomials [48]: the idea is
 137 to express the n^{th} -order polynomial fit function $f_n(y)$ in terms of orthogonal polynomials $P_k(y)$
 138 of degree $k = 0, 1, \dots, n$, instead of a parameterization in terms of monomials, $1, y, y^2, \dots, y^n$. To
 139 this aim we write

$$f_n(y) = \sum_{k=0}^n \alpha_k P_k(y), \quad \langle P_r(y) P_s(y) \rangle \propto \sum_{i=1}^{14} P_r(y_i) P_s(y_i) \propto \delta_{rs}, \quad (1)$$

140 where y_i are the values in Tab. 1. This method is equivalent to the naive one, but is numerically
 141 more stable and the fit parameters α_k can be determined with improved precision and less statistical
 142 noise.

143 The optimal degree n for the fitting polynomial is not known *a priori* and is determined in the
 144 following way: The fit with weights proportional to the inverse square of errors is done for several
 145 values of n , and the least chi-square χ_{\min}^2 is found as a function of n . At a given order \bar{n} , adding
 146 a further term $\alpha_{\bar{n}+1} P_{\bar{n}+1}$ results in a negligible change of χ_{\min}^2 and the best fit yields a result for

²Note that the lower quality of $3 > d > 2$ data is due to the coarse scanning of Δ_σ values, not to an intrinsic limitation of the numerical bootstrap approach [19].

147 $\alpha_{\bar{n}+1}$ which is compatible with zero within errors. This identifies \bar{n} as the degree of the optimal
 148 polynomial. Finally, we use the results of our best fit for $\{\alpha_k\}$ to assign an error to $f_n(y)$ in the
 149 whole range of $4 > d \geq 3$. Details on the fitting procedure and the computation of errors can be
 150 found in App. A.

151 In this section we focus on the three leading operators σ, ϵ and ϵ' (corresponding to ϕ, ϕ^2 and
 152 ϕ^4 in the ϕ^4 field theory), which are determined with very good precision. The analysis of higher-
 153 dimensional operators is postponed to Sec. 4.2. Instead of working with conformal dimensions, we
 154 consider the anomalous dimensions

$$\gamma_\sigma = \Delta_\sigma - \frac{d-2}{2}, \quad \gamma_\epsilon = \Delta_\epsilon - (d-2), \quad \gamma_{\epsilon'} = \Delta_{\epsilon'} - 2(d-2). \quad (2)$$

155 They are related to the Ising critical exponents η, ν and ω by

$$\eta = 2\gamma_\sigma, \quad \frac{1}{\nu} = 2 - \gamma_\epsilon, \quad \omega = d - 4 + \gamma_{\epsilon'}. \quad (3)$$

156 The vanishing of anomalous dimensions in the free theory ($d = 4$) is assumed in the following fits.

157 Our analysis starts by comparing the old [19] and new data for $4 > d > 3$. In Fig. 3 the new
 158 results (blue circles) show much smaller errors than the earlier findings (red crosses), due to a more
 159 accurate localization of the Ising point, as explained above. In these and later figures we report the
 160 differences ($\gamma_{\mathcal{O}} - \text{fit}$) between data and fitting polynomial, because simpler plots would not capture
 161 the small errors involved. (Note that the abscissas of the three plots differ by factors of ten). The
 162 explicit form of the best fitting polynomials are provided in Sec. 3.

163 The relative errors of our data, determined from Tab. 1 and the figures, can be summarized as
 164 follows:

$$\frac{\text{Err}(\gamma_\sigma)}{\gamma_\sigma} \approx \frac{\text{Err}(\gamma_\epsilon)}{\gamma_\epsilon} \approx \frac{\text{Err}(\Delta_{\epsilon'})}{\Delta_{\epsilon'}} \approx 0.001, \quad 3.875 \geq d \geq 3. \quad (4)$$

165 Given the small size of anomalous dimensions for $d \rightarrow 4$, these correspond to extremely low absolute
 166 errors, $\text{Err}(\gamma_\sigma) = O(10^{-6})$ and $\text{Err}(\gamma_\epsilon) = O(10^{-5})$ in this range, as spelled out in the following
 167 sections. This is one of the main results of our work. It allows us to perform a precise comparison
 168 to other methods, and the determination of benchmark values for the Ising universality class in
 169 non-integer dimensions.

170 It is interesting to compare our results with those recently reported in Ref. [20], obtained by
 171 solving a 3-correlator bootstrap with the navigator method. In Fig. 4 we plot our data in earlier
 172 figures (blue circles) on a finer scale together with the estimated error of the fit (cyan shaded area).
 173 The results of [20] are drawn as red triangles: although such determinations come with no error
 174 bar, the comparison in Fig. 4 clearly shows the very good agreement between the two different
 175 bootstrap approaches at our precision level. A qualitative indication of 3-correlator data errors is
 176 given by their known values at $d = 3$ with *rigorous bounds* [46, 49], that are plotted in Fig. 4 as
 177 black diamonds (γ_σ and γ_ϵ) and grey rightward triangle ($\gamma_{\epsilon'}$) respectively: their size confirms the
 178 consistency between results.

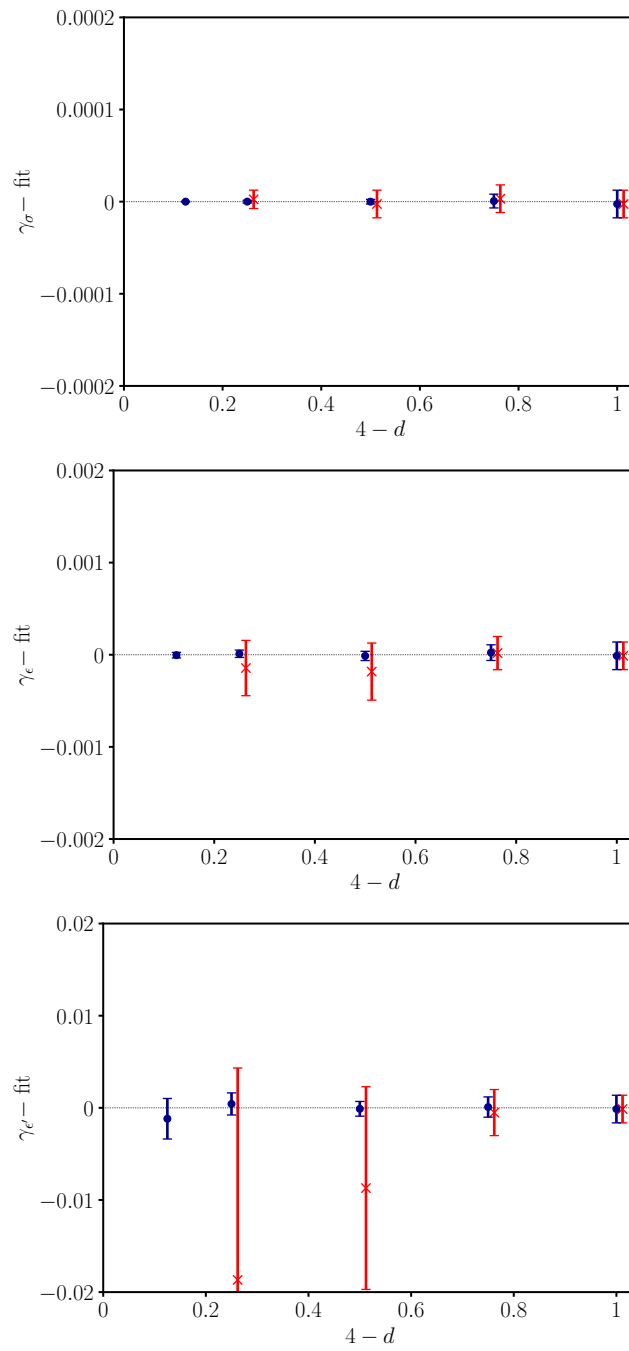


Figure 3: Old [19] (red crosses) and new (blue circles) bootstrap data for $\gamma_\sigma, \gamma_\epsilon, \gamma_{\epsilon'}$, minus the corresponding best fits. The plots use the same scales as in Ref. [19].

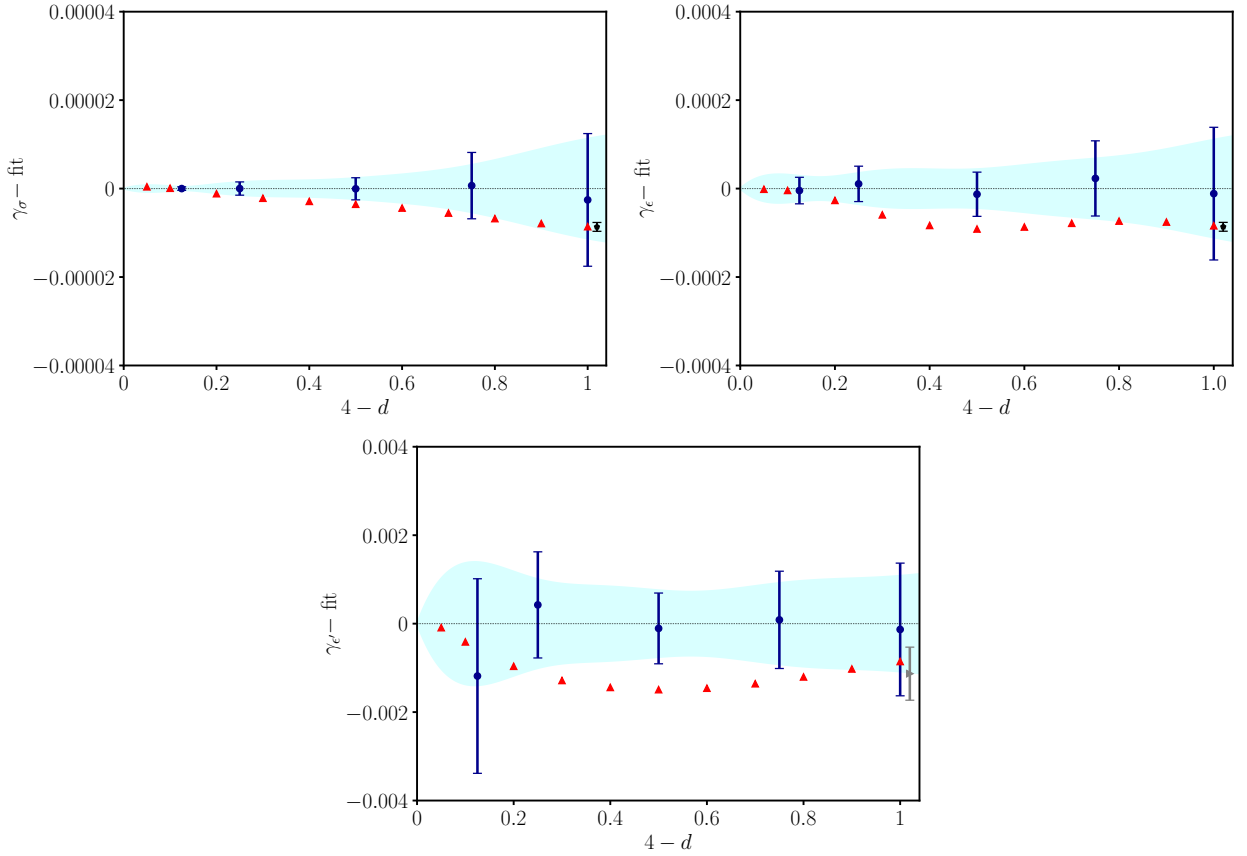


Figure 4: Plot of bootstrap data for $\gamma_\sigma, \gamma_\epsilon, \gamma_{\epsilon'}$ minus the best fit values. The shaded area represents the error obtained from the χ^2 minimization of the fitting polynomial. The red triangles are results from Ref. [20] using the navigator method in a 3-correlator bootstrap setup; these points have no error bar. Black diamonds and grey rightward triangle represent respectively results for $d = 3$ from Ref. [46] (γ_σ and γ_ϵ) and Ref. [49] ($\gamma_{\epsilon'}$); these data points are slightly displaced around $d = 3$ to improve readability.

179 3 Comparison with the epsilon expansion in $4 > d \geq 3$

180 In this section, we recall some features of the epsilon expansion and the resummation methods
 181 employed for it. We compare unresummed and resummed series with the bootstrap results for γ_σ .
 182 Then, the analysis is extended to γ_ϵ and $\gamma_{\epsilon'}$.

183 3.1 Warm-up analysis of the anomalous dimensions γ_σ

184 We start with a brief summary of the properties of the perturbative expansion of the ϕ^4 field
 185 theory in $d = 4 - y$, which describes the Ising universality class. This is a textbook subject [50]
 186 but we would like to single out a few aspects that are important in the following comparison with
 187 bootstrap results in varying dimensions³.

188 The β -function $\beta(g, y)$ and the anomalous dimensions $\gamma_{\mathcal{O}}(g)$, where $\mathcal{O} = \phi, \phi^2, \phi^4$, take the

³An up-to-date discussion of epsilon expansion can be found in Refs. [36–39]. We refer to these works for a proof of the following statements and appropriate referencing.

189 following form, in the Minimal Subtraction (MS) [50, 51] renormalization scheme,

$$\beta(g, y) = -yg + \sum_{k=2}^{n+1} \beta_k g^k, \quad \gamma_{\mathcal{O}}(g) = \sum_{k=1}^n \gamma_{\mathcal{O},k} g^k. \quad (5)$$

190 The numerical coefficients $\beta_k, \gamma_{\mathcal{O},k}$ were computed up to order $n = 6$ in Ref. [38], and $n = 7$ in
 191 Ref. [52]. While results up to order $n = 15$ are known for a subclass of Feynman diagrams believed
 192 to give the dominant contribution, they are not used here [38, 53].

193 The coefficients of the β -function (5) grow exponentially with k , and their asymptotic behavior
 194 can be estimated from the contribution of instanton field configurations [50]

$$\beta_k \underset{k \rightarrow \infty}{\sim} C (-a)^k k^b k!. \quad (6)$$

195 Similar behaviors are found for the coefficients $\gamma_{\mathcal{O},k}$. The parameters a, b, C depend on the quantity
 196 considered. One finds that the known values of the coefficients up to order $n = 7$ grow very fast
 197 with n but have not yet reached their asymptotic values (6) [38, 53].

198 The behavior (6) can be understood as follows: The perturbative series has a vanishing radius
 199 of convergence in the complex g plane, because real negative values of g correspond to an upside-
 200 down potential and an action not bounded from below. This fact can be exemplified by the simple
 201 *zero-dimension path integral* (see App. B):

$$\mathcal{I}(g) = \int_{-\infty}^{\infty} \frac{dx}{\sqrt{2\pi}} e^{-\frac{x^2}{2} - gx^4} = \sum_{k=0}^{\infty} a_k (-g)^k, \quad a_k = \frac{(4k)!}{2^{2k}(2k)!k!} \underset{k \rightarrow \infty}{\sim} \frac{2^{4k}}{\sqrt{2\pi}k} \times k!. \quad (7)$$

202 This is the generating function counting the number of vacuum Feynman diagrams. The asymp-
 203 totic behavior of a_k can be found by a saddle-point analysis of the integral. In field theory the
 204 corresponding saddle point is given by instantons [50]⁴.

205 The solution of the fixed-point equation $\beta(g, y) = 0$ gives $g = g(y)$ by perturbative inversion
 206 around $g = y = 0$; this is used to rewrite the anomalous dimensions as a series in y ,

$$\gamma_{\mathcal{O}}(y) = \sum_{k=1}^n \bar{\gamma}_{\mathcal{O},k} y^k. \quad (8)$$

207 This is again a divergent series of asymptotic form (6), with suitable parameters a, b and C .

208 The ratio of two consecutive terms in the series (8) can be estimated from (6) as, $\bar{\gamma}_{\mathcal{O},k} y / \bar{\gamma}_{\mathcal{O},k-1} \approx$
 209 $-ak y$, which is larger than one for $y > 1/|ak|$. A simple conclusion is that the more terms are
 210 present in the perturbative series (8), the sooner it diverges as a series in y . We can draw two main
 211 conclusions:

- 212 *i)* As it stands, the perturbative series (8) is basically useless for physical dimension $y = 1$,
 213 apart from the first couple of terms, and resummation methods are necessary for extracting
 214 precise values of anomalous dimensions. The resummation is based on the Borel transform,
 215 followed by a conformal mapping, as will be explained later, and further discussed in App. B.
 216 This procedure gives resummed finite expressions $\tilde{\gamma}_{\mathcal{O}}(y)$.

⁴There is growing consensus that the large-order behavior is governed by an instanton rather than a renor-
 malon [53]. If one could go to much higher orders in the series expansion (e.g., 20-loop order) one could apply
 methods of resurgence and trans-series [54].

217 *ii)* For dimensions close to $d = 4$, i.e., $y \ll 1$, there is an optimal number of terms $n_{\text{opt}}(y)$, for
 218 each y value, for which the distance between the series and the resummed function $\tilde{\gamma}_{\mathcal{O}}(y)$,
 219 $|\tilde{\gamma}_{\mathcal{O}}(y) - \sum_1^{n_{\text{opt}}} \bar{\gamma}_{\mathcal{O},k} y^k|$, is minimal before growing again.

220 The perturbative anomalous dimensions $\tilde{\gamma}_{\mathcal{O}}$ may differ from results obtained by other methods,
 221 such as the lattice formulation of the path-integral for the Ising model, or by the bootstrap. These
 222 differences are non-analytic, e.g., $\delta\gamma_{\mathcal{O}}(y) \sim \exp(-A/y)$. Within the resummation procedure, these
 223 terms may change according to how the inverse Borel transform is performed [54].

224 Before discussing the resummation methods in the next section, a first comparison of the per-
 225 turbative expansion and the bootstrap data for γ_{σ} clarifies the issues at stake.

226 The perturbative series is [38, 52]

$$\begin{aligned} \gamma_{\sigma}(y) = & 0.00925926y^2 + 0.00934499y^3 - 0.00416439y^4 + 0.0128282y^5 \\ & - 0.0406363y^6 + 0.15738y^7, \quad (\text{epsilon expansion}). \end{aligned} \quad (9)$$

227 The best polynomial fit of bootstrap data in Tab. 1 using the methods outlined in Sec. 2.2 is⁵

$$\begin{aligned} \gamma_{\sigma}(y) = & 0.009306473y^2 + 0.008899908y^3 - 0.001435107y^4 + 0.001788710y^5 \\ & - 0.000533980y^6 + 0.000128667y^7, \quad (\text{conformal bootstrap}). \end{aligned} \quad (10)$$

228 The two polynomials (9) and (10) have different meanings, although their first two coefficients
 229 are close. On one hand the Feynman-diagram series is exact, but has a vanishing radius of con-
 230 vergence. On the other hand, the numerical bootstrap data in Tab. 1 should converge to exact
 231 non-perturbative results upon increasing the numerical precision. The collection of these values
 232 for any dimension $d = 4 - y$ gives the exact function $\gamma_{\sigma}^{\text{ex}}(y)$, which however cannot be expressed
 233 in terms of a simple polynomial. Therefore, the fit (10) gives approximated values around $\gamma_{\sigma}^{\text{ex}}(y)$,
 234 whose precision is *a priori* limited. Nonetheless, this description is sufficient at the present level of
 235 numerical accuracy.

236 In Fig. 5 we show the difference between the perturbative series (9) and the bootstrap fit (10)
 237 for $4 > d \geq 3$. Color lines correspond to the series (9) truncated at different orders $n = 2, 3, \dots, 7$
 238 (cf. color legend in the plot). One sees that, the higher the order $n \geq 4$, the sooner the perturbative
 239 series diverges from the bootstrap data (corresponding to the zero horizontal line in Fig. 5). The
 240 tiny errors of bootstrap points cannot be seen at this scale, thus showing that the unresummed
 241 perturbative series cannot be used for a precise determination of critical exponents in $d = 3$, as
 242 stated in point *ii)* above. Yet, the lower terms $n = 2, 3$ may provide crude estimates.

243 Fig. 6 shows the other regime, close to four dimensions. Only the bootstrap point for $d = 3.875$ is
 244 present in this range, but we also show results of Ref. [20] for $d \geq 3.8$, which match very well while
 245 lacking error bars⁶. In contrast to the $d \approx 3$ region, we observe that the truncated perturbative
 246 series shows a different behavior. At any given y value, upon increasing the perturbative order up
 247 to an optimal value $n_{\text{opt}} \sim 1/y$, the perturbative series approaches the zero horizontal line (with a
 248 cyan error band), before starting to diverge. Namely, it matches the exact bootstrap value $\gamma_{\sigma}^{\text{ex}}(y)$,
 249 within numerical errors.

⁵Note that the best-fit polynomial (10) starts with an $O(y^2)$ term, because the linear term vanishes within errors. If a linear term is included in the fit procedure, it leads to a coefficient three orders of magnitude smaller than the quadratic term. Therefore, the conformal bootstrap implies $\gamma_{\sigma}(y) = O(y^2)$ close to $d = 4$, in agreement with perturbation theory.

⁶Note that the red triangles are not used in our fit of bootstrap data.

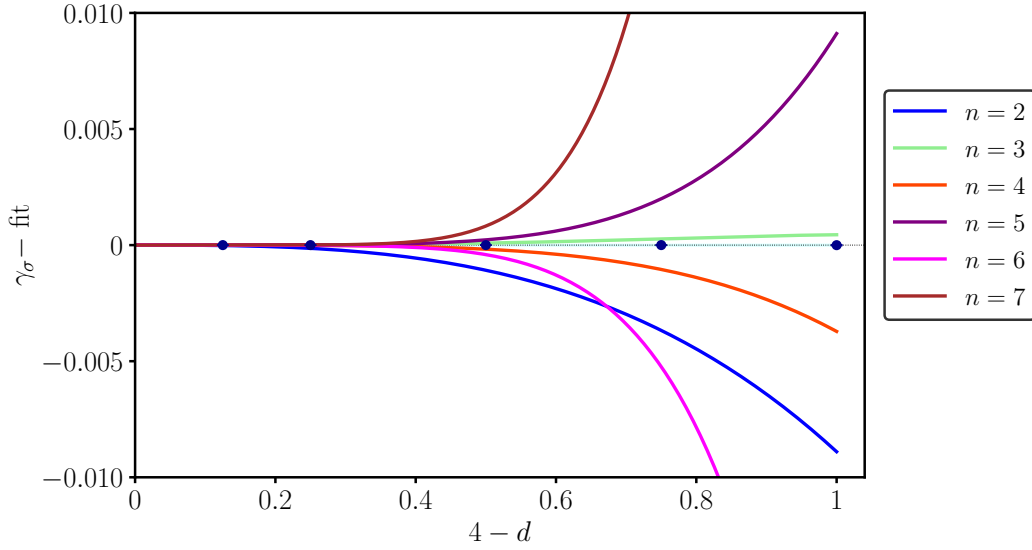


Figure 5: Comparison of γ_σ bootstrap data with unresummed epsilon expansion (9) in the region $4 > d > 3$ for truncations of the series to order $n = 2, \dots, 7$ (see color legend). All quantities have been subtracted by the best fit values (see (10)).

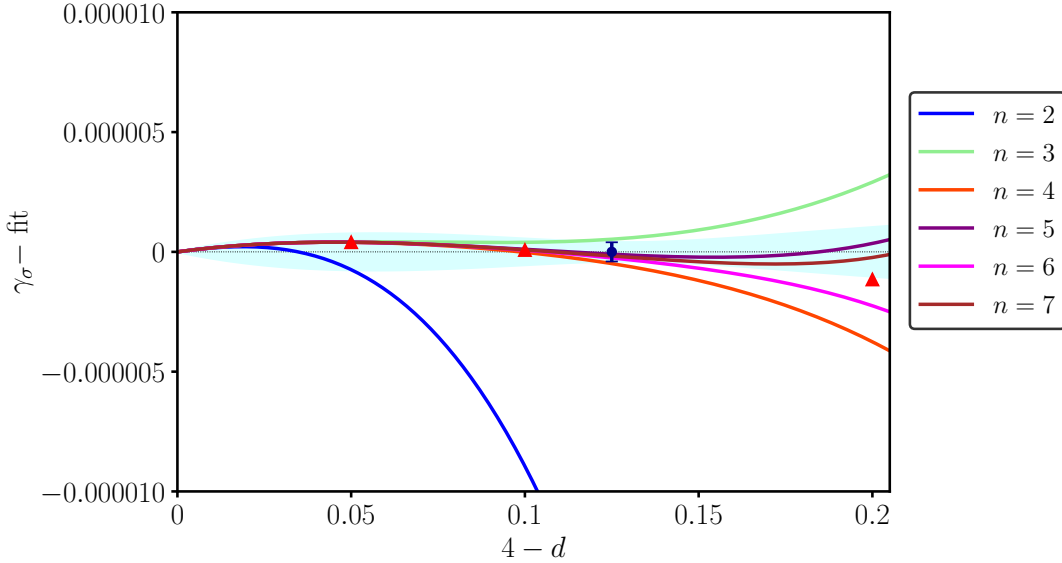


Figure 6: Comparison of γ_σ data minus best fit in the region $4 > d > 3.8$, between bootstrap (blue circle) and unresummed epsilon expansion (9) with different truncations of the perturbative series (cf. Fig. 5). The red triangles are the results of the bootstrap navigator method [20]. The cyan shaded area is the fit error.

250 Therefore, the comparison between non-perturbative bootstrap results and unresummed epsilon
 251 expansion for $\gamma_\sigma(y)$ is extremely good in the region $4 > d > 3.8$, with precision $\text{Err}(\gamma_\sigma) \approx 1 \times 10^{-6}$,
 252 i.e., $\text{Err}(\gamma_\sigma)/\gamma_\sigma < 1 \times 10^{-3}$. According to the previous discussion, we conclude that we do not see
 253 any non-perturbative difference for $d \rightarrow 4$.

254 We remark that the epsilon expansion can also be obtained by analytic solution of the bootstrap

255 equations around $d = 4$, assuming a perturbative expansion near the free theory [23,24,26,27,29–31].
 256 Thus, is our comparison in Fig. 6 tautological? It is not, because the bootstrap identity is a set of
 257 consistency conditions that depends on the kind of quantities they act on. Our numerical solution
 258 does not assume any perturbative expansion, i.e., it is an independent solution of the bootstrap
 259 constraints. That without any perturbative input, our conformal bootstrap results accurately
 260 reproduce perturbative predictions close to $d = 4$ is non-trivial.

261 A natural question is how our numerical bootstrap approach can reproduce the perturbative
 262 series, i.e., in which regime the two polynomials (9) and (10) may agree beyond the $O(y^3)$ term. As
 263 said earlier, the bootstrap polynomial (10) is approximated, it can at most describe a band of values
 264 around $\gamma_\sigma^{\text{ex}}(y)$. While the size $\text{Err}(\gamma_\sigma)$ of this band stays finite in the whole range $0 < y < 1$ (see
 265 plots), that of the epsilon expansion is expanding in y and can be finite only for $y < y_{\text{max}} \sim O(1/n)$,
 266 n being the perturbative order. We expect that, upon running the bootstrap for several points y_i ,
 267 with $0 < y_i < y_{\text{max}} \ll 1$, and by performing best fits with polynomials limited to such a small
 268 interval, one may find that the two expressions (9) and (10) match order by order, i.e., the epsilon
 269 expansion is fully recovered.

270 3.2 Bootstrap data versus resummed perturbative results

271 Precise estimates of the critical exponents have been obtained over the years by refining the
 272 resummation techniques applied to the epsilon expansion series [2–4,38,39,50,55,56]. In this work,
 273 we use the methods of Refs. [38,39] extended to dimension $4 > d \geq 3$. Let us briefly recall the main
 274 steps involved [50]. The Borel transform $\mathcal{B}_{\gamma_\mathcal{O}}(t)$ of the perturbative expansion for the anomalous
 275 dimension $\gamma_\mathcal{O}$ (8) is defined by removing the factorial growth from the series,

$$\mathcal{B}_{\gamma_\mathcal{O}}(t) = \sum_{k=1}^n \frac{\tilde{\gamma}_{\mathcal{O},k}}{k!} t^k. \quad (11)$$

276 One infers from the asymptotic behavior (6) that this function has a singularity $\mathcal{B}_{\gamma_\mathcal{O}}(t) \sim (1 +$
 277 $ta)^{-b-1}$ and a corresponding finite radius of convergence.

278 The resummed quantity is defined by the inverse Borel transform,

$$\tilde{\gamma}_\mathcal{O}(y) = \int_0^\infty dt e^{-t} \mathcal{B}_{\gamma_\mathcal{O}}(yt). \quad (12)$$

279 By definition $\gamma_\mathcal{O}(y)$ in (8) and $\tilde{\gamma}_\mathcal{O}(y)$ in (12) have the same perturbative expansion; however, the
 280 latter should be better behaved if $\mathcal{B}_{\gamma_\mathcal{O}}(t)$ is suitably continued analytically outside the original disc
 281 $|t| < 1/|a|$ to a region including the real positive axis⁷. Such analytic continuation in principle
 282 requires the knowledge of all singularities of $\mathcal{B}_{\gamma_\mathcal{O}}(t)$ in the complex t -plane. At this point, one can
 283 only make educated guesses on these singularities, that translate into (physical) ansatzes for $\tilde{\gamma}_\mathcal{O}(y)$.

284 In practice, one assumes that the only singularity of $\mathcal{B}_{\gamma_\mathcal{O}}(t)$ lies at $t = -1/a$ real and negative,
 285 and that it is a branch cut extending to $t = -\infty$. Using a conformal mapping $t(z)$, this branch cut
 286 is mapped onto the unit circle, with the start of the branch cut mapped onto $z = -1$, and $t = -\infty$
 287 to $z = 1$, preserving the origin $z = t = 0$. As long as there are no other singularities, $\mathcal{B}(t(z))$ has
 288 a radius of convergence one in z . As $t = \infty$ corresponds to $z = 1$, this allows one to perform the
 289 inverse Borel transform (12). Details on this procedure can be found in App. B.

⁷In particular, a real negative value of the parameter a in (6), i.e., a perturbative series (8) of definite sign, is problematic.

290 This general idea can be modified in several ways, allowing one to introduce a set of variational
 291 parameters. The latter are determined such that the final result is the least sensible to their
 292 variation. Apart from providing a robust resummation scheme, it allows one to obtain an estimate
 293 of the error in the resummation. These methods have been improved over the years by taking into
 294 account the phenomenology of critical phenomena.

295 Let us also mention that another appealing option for the analytic continuation is to use Hyperge-
 296 ometric functions, for which the inverse Borel transform can be written as a Meijer-G function [55].
 297 One drawback of this approach is the possibility for spurious poles on the integration contour.

298 Figure 7 shows the fitted bootstrap data (blue points) of $\gamma_\sigma(y)$ already reported in Fig. 4, now
 299 compared to the resummed epsilon-expansion values of Tab. 2 (green squares)⁸. The agreement
 300 between these two results is very good, especially for $d \geq 3.5$, where the unresummed series (ma-
 301 genta line) is already diverging, and greatly improves on earlier studies [2, 3] analyzed in [19]. Let
 302 us remark that resummed $\tilde{\gamma}_\sigma(y)$ values have been obtained for non-integer dimensions down to
 303 $d = 2$, still finding agreement with bootstrap data, although with larger uncertainties. Finally,
 304 Fig. 7 shows the latest Monte Carlo results in $d = 3$ (yellow rhombus), that match extremely well
 305 the bootstrap points. Further $d = 3$ results by these and other methods are summarized in a later
 306 figure.

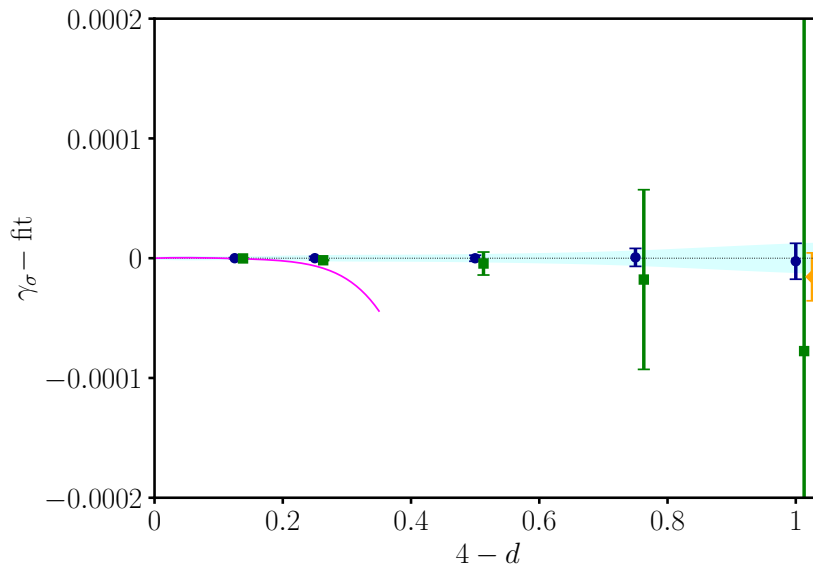


Figure 7: Comparison of γ_σ data minus best-fit values: bootstrap (blue circles), Borel-resummed epsilon expansion [38] (green squares), unresummed high-order epsilon expansion (magenta solid curve), $d = 3$ Monte Carlo [42] (yellow rhombus). Note that data points are slightly displaced around the same d values ($d = 3.875$, $d = 3.75$, $d = 3.5$, $d = 3.25$ and $d = 3$) to improve readability.

⁸Resummations in this section use the 6th-order expansion that received several checks. Contrary to expectation, the apparent error at 7-loop order seems to be larger than that at 6-loop order, in all resummation schemes we tried [38, 39]

d	Δ_σ	Δ_ϵ	Δ'_ϵ
3.875	0.937662197(7)	1.91831086(14)	3.9924550(11)
3.75	0.8757158(3)	1.839419(4)	3.97529(3)
3.5	0.753393(10)	1.68854(7)	3.9276(5)
3.25	0.63386(8)	1.5458(4)	3.873(2)
3	0.5181(3)	1.4108(12)	3.820(7)

Table 2: Conformal dimensions of σ, ϵ and ϵ' field from resummed perturbative expansion, obtained according to the methods of [38].

307 We now extend the previous analysis to the energy field ϵ . The best fit of the conformal bootstrap
308 data is

$$\begin{aligned} \gamma_\epsilon(y) = & 0.333441601y + 0.114095325y^2 - 0.083458310y^3 \\ & + 0.081381007y^4 - 0.045296977y^5 + 0.014290102y^6 \\ & - 0.001741325y^7, \end{aligned} \quad (\text{conformal bootstrap}). \quad (13)$$

309 The epsilon-expansion series reads [38, 52]

$$\begin{aligned} \gamma_\epsilon(y) = & 0.333333y + 0.117284y^2 - 0.124527y^3 + 0.30685y^4 - 0.95124y^5 \\ & + 3.57258y^6 - 15.2869y^7, \end{aligned} \quad (\text{epsilon expansion}). \quad (14)$$

310 One remarks the agreement, within errors, of the first two coefficients of this series; this corrects
311 less precise results of [19] (cf. Fig. 6b there).

312 The comparison for $d \rightarrow 4$ before resummation is shown in Fig. 8. As for Fig. 7, the truncated
313 perturbative series for γ_ϵ are plotted. Their curves approach the bootstrap fit (horizontal zero
314 axis with cyan error band) with better and better precision. Note the remarkable quality of the
315 navigator method (red triangles) [20]. Altogether, the agreement for $d \rightarrow 4$ is found with high
316 precision, $\text{Err}(\gamma_\epsilon) = 3 \times 10^{-5}$ and $\text{Err}(\gamma_\epsilon)/\gamma_\epsilon = 1 \times 10^{-3}$.

317 Figure 9 presents a comparison with the resummed perturbative series (Tab. 2): the agreement
318 is again very good for $4 > d \geq 3.5$; there is a small $O(10^{-3})$ deviation from the bootstrap and
319 Monte Carlo results [42] (yellow rhombus) in $d = 3$. Probably there is a slight underestimation of
320 the error. Let us remark that this resummation procedure is *honest*, as it does not use the exact
321 $d = 2$ conformal dimension as an input, with which it could be improved. The comparison with
322 another method, called Self-Consistent (SC) resummation⁹ is presented in Fig. 10, where we plot
323 data of Tab. 3. In this case, the Borel transform is done on the perturbative series of $1/\nu^3$, instead
324 of $1/\nu = 2 - \gamma_\epsilon$: this choice is motivated by a match with the $d = 2$ conformal field theory, that is
325 achieved through comparing the n dependence of the $O(n)$ -symmetric ϕ^4 theory [39]. We conclude
326 that adding information of the exact results in $d = 2$ improves the resummation of the perturbative
327 series (for this particular critical exponent).

328 Summarizing, the bootstrap and epsilon-expansion results agree very well: for $d \rightarrow 4$ the unre-
329 summed series fits perfectly, for $4 > d \geq 3$ there is remarkable agreement, keeping in mind that
330 the resummation error is roughly one order of magnitude larger than that of bootstrap and Monte
331 Carlo results.

⁹See Ref. [39] for a detailed discussion of this approach.

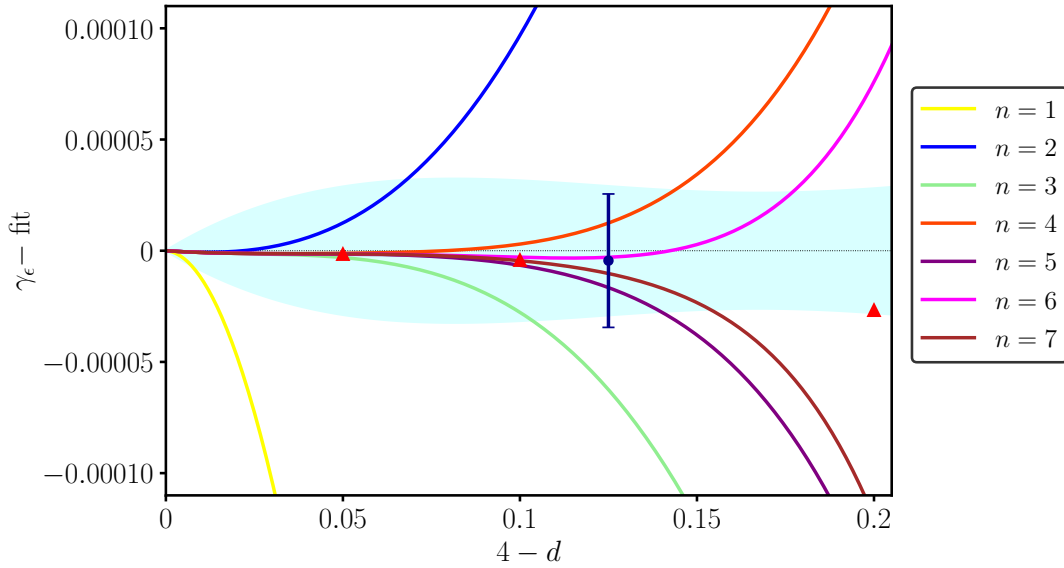


Figure 8: Comparison of the γ_ϵ data minus the best fit in the region $4 > d > 3.8$. Our bootstrap point is the blue circle with error bar; the triangles are obtained by the navigator method [20]; the different truncations of the perturbative series are as in Fig. 5. The cyan shaded area is the fit error.

d	Δ_ϵ
3.9	1.93440534057(12)
3.8	1.8706742(6)
3.7	1.808546(5)
3.6	1.747876(2)
3.5	1.68858(6)
3.4	1.63062(15)
3.3	1.5740(3)
3.2	1.5187(5)
3.1	1.4647(9)
3	1.4122(15)

Table 3: Conformal dimension of ϵ field from resummed perturbative expansion, obtained according to the methods of [39].

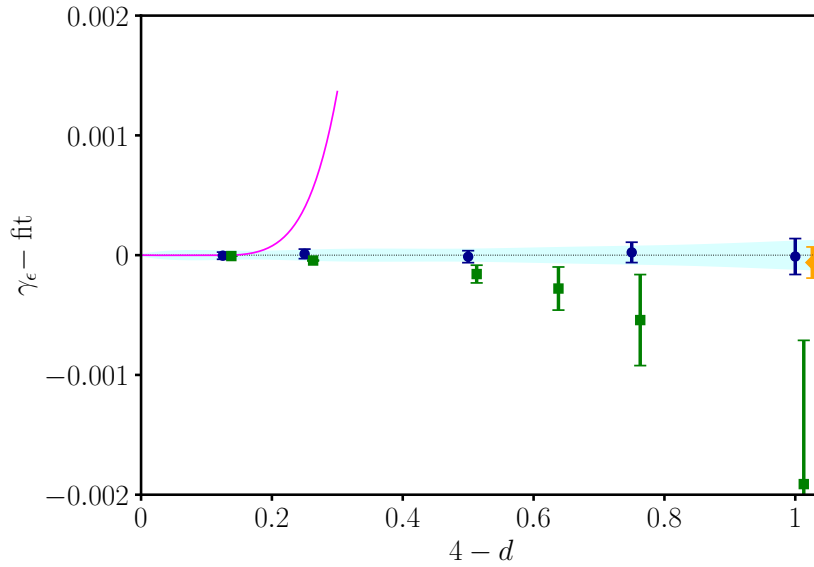


Figure 9: Comparison of γ_ϵ data minus best fit: bootstrap (blue circles), Borel-resummed epsilon expansion [38] (green squares), unresummed epsilon expansion (magenta solid curve), $d = 3$ Monte Carlo [42] (yellow rhombus). The cyan shaded area is the fit error as in earlier plots.

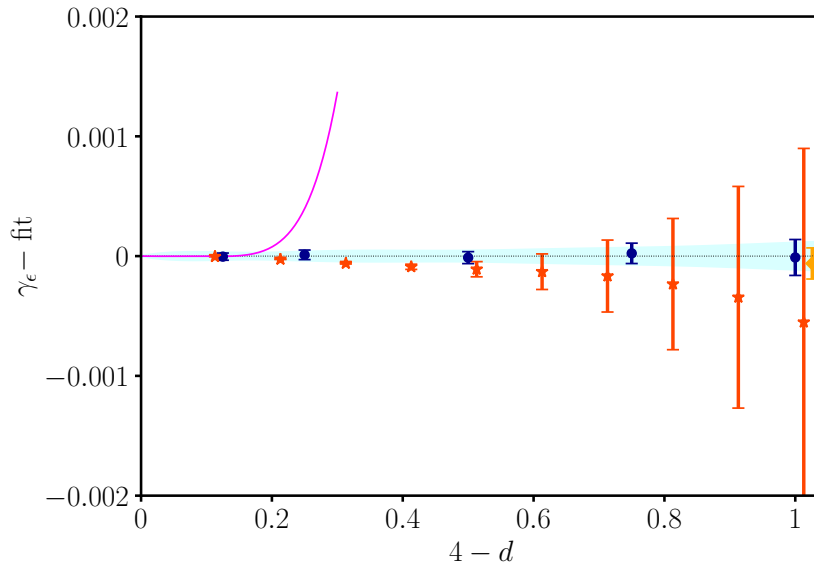


Figure 10: Comparison of γ_ϵ minus best fit: bootstrap (blue circles), Self-Consistent resummed epsilon expansion [39] (red stars), unresummed epsilon expansion (magenta solid curve), $d = 3$ Monte Carlo [42] (yellow rhombus).

332 A comparison of all $d = 3$ results available in the literature for γ_σ and γ_ϵ is given in Figs. 11
 333 and 12. The corresponding numerical values are in Tab. 4. Besides data already discussed (drawn
 334 in earlier colors), we report recent results of the non-perturbative renormalization group [43] (brown
 335 downward triangle). The central value is given by our fit of the bootstrap data with error given by
 336 the cyan band, not by the mean value of all results. The Figs. 11 and 12 respect our convention
 337 of plotting the two anomalous dimensions on scales differing by one order of magnitude, roughly
 338 equal to the ratio of their actual value. Finally, Tab. 4 and Figs. 11, 12 report also the results
 339 of other 3-correlator bootstrap approaches, using EFM [46] and the navigator method [49], and
 340 paying particular attention to error estimates (cf. rigorous bounds). We also remark that the
 341 results obtained by perturbative expansions directly in $d = 3$ [3, 4] are consistent with bootstrap
 342 results too, but have one order of magnitude larger errors and are therefore not plotted in Figs. 11
 343 and 12.

$d = 3$ Ising critical indices	Δ_σ	Δ_ϵ	$\Delta_{\epsilon'}$
Bootstrap (1 correlator)	0.518155(15)	1.41270(15)	3.8305(15)
Bootstrap (3 correlators)	0.5181489(10)	1.412625(10)	3.8297(2)
Borel resummed epsilon expansion	0.5181(3)	1.4107(13)	3.820(7)
SC Borel resummed epsilon expansion	0.5178(2)	1.4122(15)	3.827(13)
Monte Carlo	0.51814(2)	1.41265(13)	3.832(6)
Non-perturbative RG	0.5179(3)	1.41270(50)	3.832(14)
Navigator (rigorous bounds)	0.518157(35)	1.41265(36)	3.8295(6)

Table 4: Comparison of $d = 3$ results for the conformal dimensions of low-lying fields: 1-correlator bootstrap [19], 3-correlator bootstrap [46] (errors on Δ_σ and Δ_ϵ are rigorous bounds), Borel-resummed epsilon expansion [38], Self-Consistent (SC) Borel-resummed epsilon expansion [39], Monte Carlo [40, 42], non-perturbative renormalization group [43, 44] and bootstrap navigator method with rigorous bounds [49].

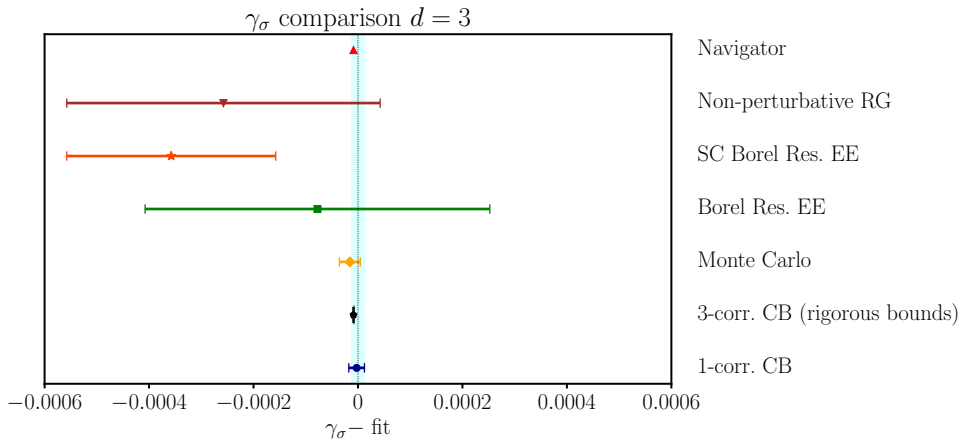


Figure 11: Summary of up-to-date predictions for γ_σ at $d = 3$ (minus best fit): 1-correlator bootstrap [19] (blue circle), 3-correlator bootstrap with rigorous bounds [46] (black pentagon), Monte Carlo [42] (yellow rhombus), Borel-resummed epsilon expansion [38] (green square), Self-Consistent resummed epsilon expansion [39] (red star), non-perturbative renormalization group [43] (brown downward triangle), bootstrap navigator method [20] (red upward triangle).

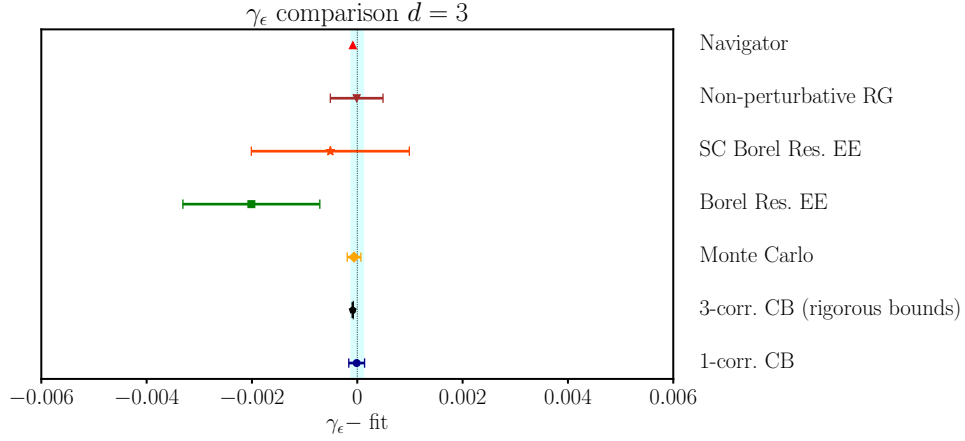


Figure 12: Summary of up-to-date predictions for γ_ϵ in $d = 3$ (minus best fit): 1-correlator bootstrap [19] (blue circle), 3-correlator bootstrap with rigorous bounds [46] (black pentagon), Monte Carlo [42] (yellow rhombus), Borel-resummed epsilon expansion [38] (green square), Self-Consistent resummed epsilon expansion [39] (red star), non-perturbative renormalization group [43] (brown downward triangle), bootstrap navigator method [20] (red upward triangle).

344 We now analyze the subleading \mathbb{Z}_2 -even scalar field ϵ' , which is related to the critical exponent
 345 $\omega = \Delta_{\epsilon'} - d = d - 4 + \gamma_{\epsilon'}$. The best fit of our data gives¹⁰:

$$\begin{aligned} \gamma_{\epsilon'}(y) = & 2.000178549y - 0.518006835y^2 + 0.721996645y^3 \\ & - 0.684437170y^4 + 0.447648598y^5 - 0.162903635y^6 \\ & + 0.026155257y^7, \end{aligned} \quad (\text{conformal bootstrap}). \quad (15)$$

346 The large errors of the earlier analysis [19] have been reduced, as explained earlier (see Fig. 3). The
 347 epsilon-expansion series is [38, 52],

$$\begin{aligned} \gamma_{\epsilon'}(y) = & 2y - 0.62963y^2 + 1.61822y^3 - 5.23514y^4 + 20.7498y^5 \\ & - 93.1113y^6 + 458.7424y^7, \end{aligned} \quad (\text{epsilon expansion}). \quad (16)$$

348 In Fig. 13 we show the difference between the data and the bootstrap best fit (15). The overall
 349 error of the fit for $\gamma_{\epsilon'}$ is estimated to be less than 2.0×10^{-3} in the whole range. The relative error
 350 is $\text{Err}(\gamma_{\epsilon'})/\gamma_{\epsilon'} = 1 \times 10^{-3}$ for $d = 3$ but goes up to 1×10^{-2} for $d = 3.875$. The comparison with
 351 Monte Carlo [40, 42] in $d = 3$, and the resummed epsilon-expansion series are also shown, finding
 352 again good agreement at the coarser scale (note a factor of 10 w.r.t. Fig. 9). A drift towards lower
 353 values for the green epsilon-expansion points is seen, as for γ_ϵ . Further values of $\Delta_{\epsilon'}$ in $d = 3$ found
 354 in the literature are reported in Tab. 4 and plotted in Fig. 14. A zoom over the region close to
 355 $d = 4$ is drawn in Fig. 15, showing the same features of Fig. 6 and Fig. 8.

356 We conclude this section by stressing the very good overall agreement of bootstrap and resummed
 357 epsilon expansion. The study in varying dimensions clarifies the different behavior of quantities in
 358 the perturbative and non-perturbative regimes.

¹⁰The fit again assumes $\gamma_{\epsilon'} = 0$ for $d = 4$.

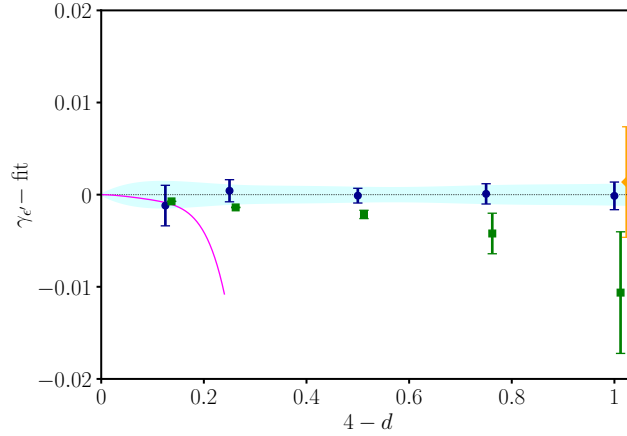


Figure 13: Comparison of $\gamma_{\epsilon'}$ data minus best fit: bootstrap (blue circles), Borel-resummed epsilon expansion [38] (green squares), unresummed epsilon expansion (magenta solid curve), $d = 3$ Monte Carlo [40] (yellow rhombus).

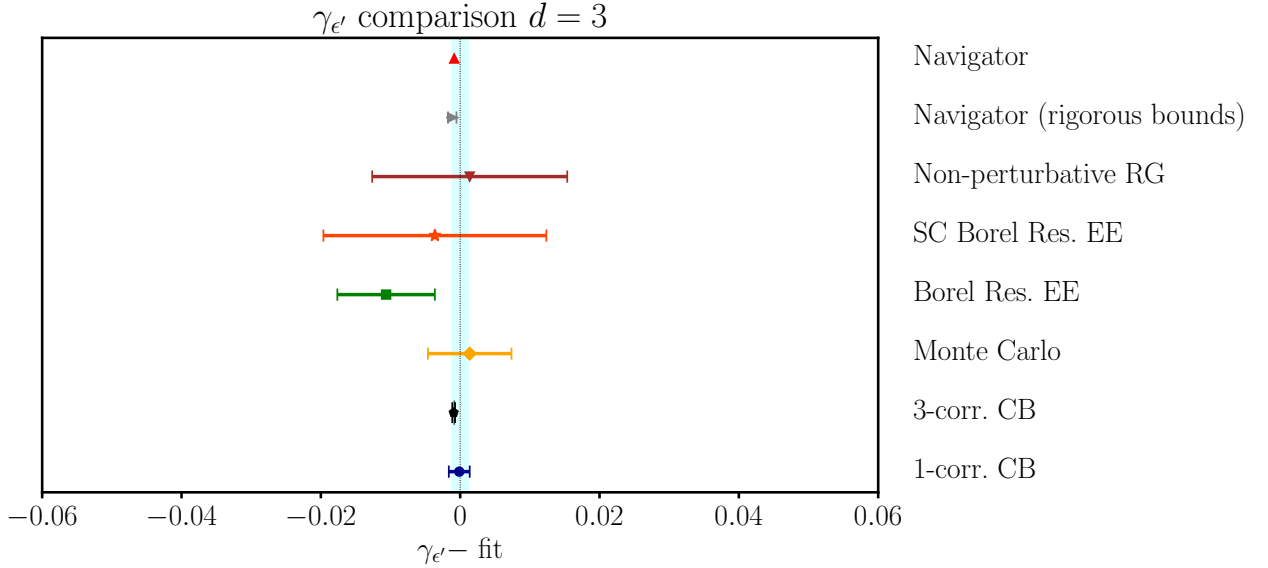


Figure 14: Summary of up-to-date predictions for $\gamma_{\epsilon'}$ in $d = 3$ (minus best fit): 1-correlator bootstrap [19] (blue circle), 3-correlator bootstrap [46] (black pentagon), Monte Carlo [42] (yellow rhombus), Borel-resummed epsilon expansion [38] (green square), Self-Consistent resummed epsilon expansion [39] (red star), non-perturbative renormalization group [43] (brown downward triangle), bootstrap navigator method with rigorous bounds [49] (grey rightward triangle), bootstrap navigator method [20] (red upward triangles).

359 4 Structure constants and scaling dimensions of higher fields

360 In this section we analyze further bootstrap data. The structure constants (OPE coefficients)
 361 of low-lying fields $\sigma, \epsilon, \epsilon', T$ are very precise, the error being on the fifth decimal, thus better than
 362 those of the corresponding conformal dimensions presented earlier. Next we discuss subleading and
 363 spinful fields, ϵ'', T', C, C' , presenting results for both dimensions and structure constants. Some of

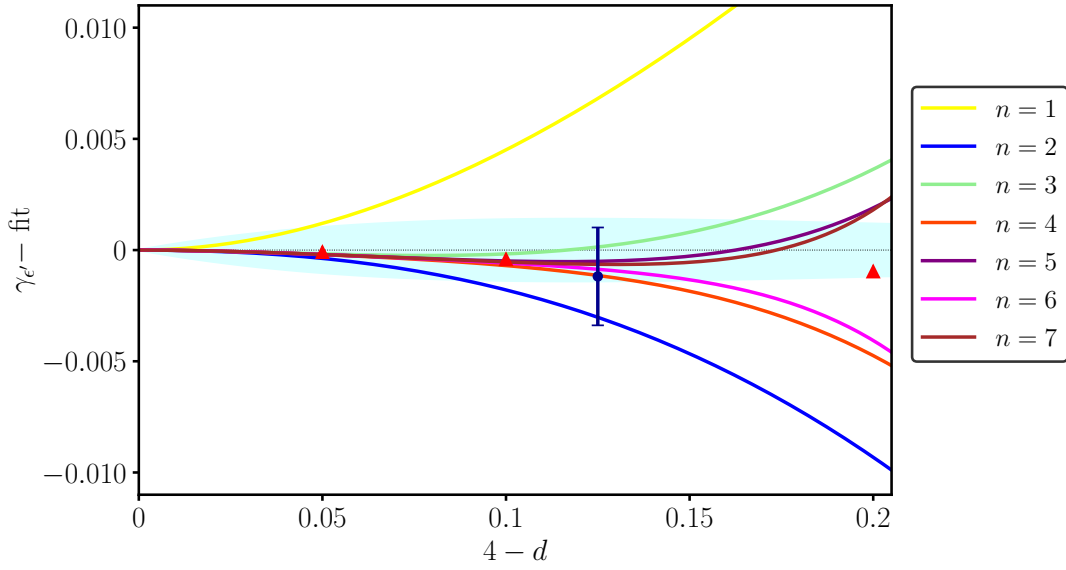


Figure 15: Comparison of the $\gamma_{\epsilon'}$ data minus the best fit in the region $4 > d > 3.8$. Our bootstrap point is the blue circle with error bar; the triangles are obtained by the navigator method [20]; the different truncations of the perturbative series are as in Fig. 5. The cyan shaded area is the fit error.

364 them are good, others are not completely correct, showing the limits of our numerical bootstrap
 365 approach.

366 **4.1 Structure constants in $4 > d \geq 3$**

d	c	$f_{\sigma\sigma\epsilon}$	$f_{\sigma\sigma\epsilon'}$	$f_{\sigma\sigma\epsilon''} \times 10^4$	$f_{\sigma\sigma T'}$	$f_{\sigma\sigma C}$	$f_{\sigma\sigma C'}$
4	1	1.4142136	0	0	0	0.169031	0
3.875	0.99970(2)	1.38228(2)	0.015298(14)	0.33(10)	0.003070(2)	0.1540603(3)	0.000772(2)
3.75	0.998594(3)	1.34586(3)	0.027517(15)	1.4(3)	0.005641(5)	0.133(8)	0.00134(10)
3.5	0.9922615(15)	1.26132(3)	0.04426(3)	4.0(2)	0.00911(10)	0.105(5)	0.0021(3)
3.25	0.976864(6)	1.16282(4)	0.05225(3)	6.0(3)	0.0106(2)	0.084(6)	0.0019(9)
3	0.946535(15)	1.05184(4)	0.05300(5)	7.1(4)	0.010575(15)	0.065(5)	0.0020(5)
2.75	0.893275(15)	0.92939(4)	0.04794(8)	7.0(4)	0.00901(6)	0.048(4)	0.00235(15)
2.5	0.807110(10)	0.796303(5)	0.03885(2)	5.90(9)	0.00668(3)	0.033(3)	0.0029(3)
2.25	0.677724(2)	0.65311(2)	0.02738(4)	4.27(5)	0.00394(14)	0.0195(15)	0.0035(2)
2.2	0.64609(7)	0.62333(6)	0.0245(5)	3.76(9)	0.00352(7)	0.019(4)	0.0038(3)
2.15	0.61243(8)	0.59313(8)	0.0225(5)	3.36(2)	0.0025(5)	0.017(3)	0.00385(15)
2.1	0.57680(10)	0.56249(7)	0.02018(8)	2.98(7)	0.00265(5)	0.016(3)	0.00395(15)
2.05	0.53935(15)	0.53143(8)	0.01785(5)	2.58(4)	0.00230(10)	0.0135(25)	0.00390(10)
2.01	0.5082(3)	0.5058(6)	0.01605(5)	2.246(9)	0.00193(3)	0.01550(10)	0.003920(10)
2.00001	0.500015(15)	0.499998(5)	0.015623(4)	2.0(2)	0.0018520(5)	0.0148235(15)	0.0039040(10)
2	0.5	0.5	0.0156250	2.1972656	0.00185290	0.0148232	0.003906

Table 5: Structure constants of the first few low-lying states for $4 > d > 2$. The exact values for $d = 2, 4$ are given in bold, results for $3 \geq d > 2$ are taken from [19].

367 Tab. 5 reports all data for structure constants: those for $4 > d > 3$ are new results, the ones for
 368 $3 \geq d > 2$ are taken from [19]. The central charge c is obtained from the structure constant $f_{\sigma\sigma T}$
 369 of the energy-momentum tensor T by

$$f_{\sigma\sigma T}^2 = \frac{d}{4(d-1)} \frac{\Delta_\sigma^2}{c}. \quad (17)$$

370 For $f_{\sigma\sigma\mathcal{O}}$, we adopt the by-now standard normalization of [20, 46]. The relation with the earlier
 371 normalization $\tilde{f}_{\sigma\sigma\mathcal{O}}$ of Ref. [15] is

$$f_{\sigma\sigma\mathcal{O}}^2 = \frac{\left(\frac{d-2}{2}\right)_\ell}{(d-2)_\ell} \tilde{f}_{\sigma\sigma\mathcal{O}}^2, \quad (18)$$

372 where $(x)_\ell \equiv \Gamma(x+\ell)/\Gamma(x)$ is the Pochhammer symbol.

373 The central charge c and the structure constants $f_{\sigma\sigma\epsilon}$ and $f_{\sigma\sigma\epsilon'}$ are determined with very high
 374 accuracy: their dependence on $y = 4 - d$ is obtained with the fit method of Sec. 3.1, assuming
 375 the exact $d = 4$ value. The resulting polynomials are reported together with the available epsilon-
 376 expansion series [29, 30, 57, 58]:

$$\begin{aligned} c(y) = & 1 - 0.015415049y^2 - 0.026663929y^3 - 0.004992140y^4 - 0.010357094y^5 \\ & + 0.007424814y^6 - 0.004670278y^7 + 0.001206599y^8, \\ & \text{(conformal bootstrap),} \end{aligned} \quad (19)$$

$$\begin{aligned} c(y) = & 1 - 0.0154321y^2 - 0.02666347y^3 \\ & - 0.0039608y^4, \\ & \text{(epsilon expansion),} \end{aligned} \quad (20)$$

377

$$\begin{aligned} f_{\sigma\sigma\epsilon}(y) = & \sqrt{2} - 0.235465537y - 0.170275458y^2 + 0.096635030y^3 - 0.113371408y^4 \\ & + 0.100586943y^5 - 0.054667196y^6 + 0.016161292y^7 - 0.001992399y^8, \\ & \text{(conformal bootstrap),} \end{aligned} \quad (21)$$

$$\begin{aligned} f_{\sigma\sigma\epsilon}(y) = & \sqrt{2} - 0.235702y - 0.168047y^2 + 0.103680y^3 - 0.224776y^4, \\ & \text{(epsilon expansion),} \end{aligned} \quad (22)$$

378

$$\begin{aligned} f_{\sigma\sigma\epsilon'}(y) = & 0.136221303y - 0.118250195y^2 + 0.067116467y^3 - 0.058700794y^4 \\ & + 0.037159615y^5 - 0.012211017y^6 + 0.001647332y^7 \\ & \text{(conformal bootstrap),} \end{aligned} \quad (23)$$

$$f_{\sigma\sigma\epsilon'}(y) = 0.1360828y + 0.11844240525y^2, \quad \text{(epsilon expansion).} \quad (24)$$

379 We remark: *i*) the excellent agreement between the first few terms of the conformal bootstrap and
 380 epsilon-expansion series, and *ii*) the need of a high-order $O(y^7, y^8)$ polynomial for precise fits. The
 381 corresponding curves are shown in Figs. 16 and 17. Note that c , $f_{\sigma\sigma\epsilon}$ and $f_{\sigma\sigma\epsilon'}$ were determined
 382 with strikingly small (relative) errors, respectively $O(10^{-5})$, $O(10^{-4})$ and $O(10^{-4})$ over the entire
 383 d range.

384 The comparison with other conformal bootstrap results is as follows: The best 3-correlator
 385 determination in $d = 3$ [46] is shown as a black pentagon in the figures. Data from the naviga-
 386 tor method [20] are also available for $f_{\sigma\sigma\epsilon}$. The agreement among different numerical setups is
 387 extremely good. Moreover, as already observed for scaling dimensions, the unresummed epsilon

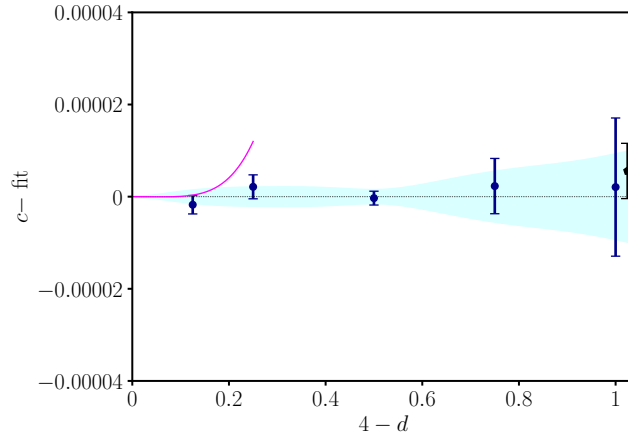


Figure 16: Comparison of c data minus best fit: bootstrap (blue circles), unresummed epsilon expansion [57, 58] (magenta solid curve), 3-correlator bootstrap at $d = 3$ [46] (black pentagon).

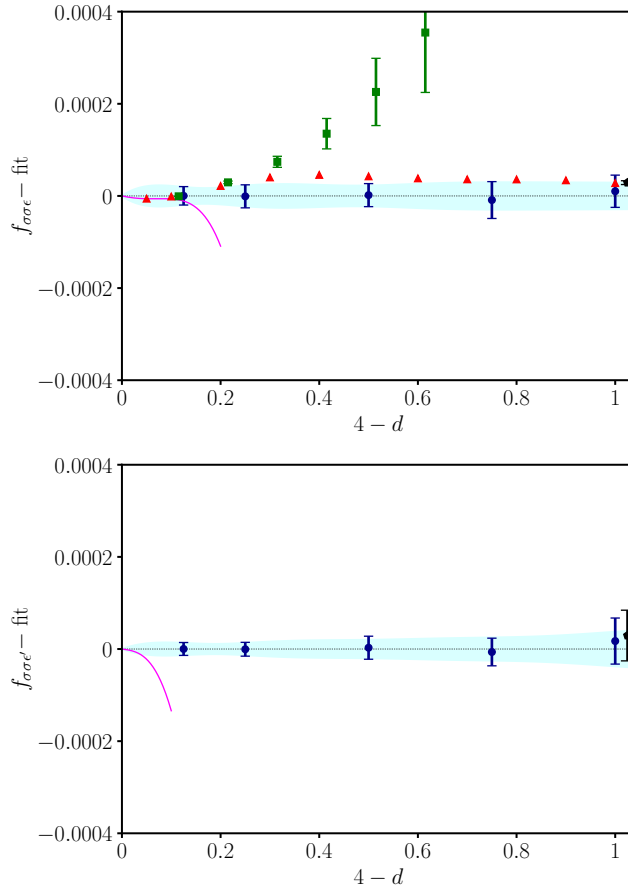


Figure 17: Comparison of $f_{\sigma\sigma\epsilon}$ and $f_{\sigma\sigma\epsilon'}$ minus best fit: bootstrap (blue circles), unresummed epsilon expansion [29, 30, 57, 58] (magenta solid curve), 3-correlator bootstrap at $d = 3$ [46] (black pentagon). On the left we also report the resummed epsilon expansion (green squares) and bootstrap navigator results [20] (red triangles).

388 expansion captures the $d \rightarrow 4$ behavior, and it does it very well, since the lower-order terms of the
 389 respective polynomials (19)–(24) are equal within errors. For $f_{\sigma\sigma\epsilon}$, the results of the resummed
 390 epsilon expansion, reported in Tab. 6, are also shown, determined by earlier methods: the 4th-order
 391 series (22) only allows for a precise agreement down to $d \approx 3.6$, given the fine scale of Fig. 17.
 392 For the remaining quantities, the epsilon expansion is either too short for a resummation, or not
 393 alternating.

d	$f_{\sigma\sigma\epsilon}$
3.9	1.3890497(2)
3.8	1.360960(3)
3.7	1.330222(12)
3.6	1.29703(3)
3.5	1.26154(7)
3.4	1.22386(13)
3.3	1.1841(2)
3.2	1.1423(3)
3.1	1.0986(5)
3	1.0531(7)

Table 6: Structure constant $f_{\sigma\sigma\epsilon}$ from resummed perturbative expansion, obtained according to the methods of [39].

394 4.2 Higher fields T' and C

395 The analysis of the fields T' ($\ell = 2$) and C ($\ell = 4$) is done along the same lines. The fit
 396 polynomials for $\Delta_{T'}$ and Δ_C , obtained as before, are

$$\begin{aligned}
 \Delta_{T'}(y) = & 6 - 0.567900778y + 0.1779633663y^2 - 0.806164966y^3 \\
 & + 1.749534636y^4 - 1.684842086y^5 + 0.765011179y^6 \\
 & - 0.126284231y^7, \quad (\text{conformal bootstrap}), \quad (25)
 \end{aligned}$$

$$\begin{aligned}
 \Delta_C(y) = & 6 - 1.001598184y + 0.030791232y^2 \\
 & - 0.033868719y^3 + 0.041665026y^4 - 0.002907562y^5 \\
 & - 0.006602770y^6, \quad (\text{conformal bootstrap}). \quad (26)
 \end{aligned}$$

397 They are shown in Fig. 18, along with the bootstrap results of [20] (red triangles) and the available
 398 epsilon-expansion series (magenta solid lines) [26, 31, 57, 58]:

$$\Delta_{T'}(y) = 6 - 0.5555556y, \quad (\text{epsilon expansion}), \quad (27)$$

$$\begin{aligned}
 \Delta_C(y) = & 6 - y + 0.01296296y^2 + 0.01198731y^3 \\
 & - 0.006591585y^4, \quad (\text{epsilon expansion}). \quad (28)
 \end{aligned}$$

399 As shown by the cyan band, representing our fitting error, the scaling dimensions of these fields are
 400 determined with an accuracy comparable to that achieved for the low-lying $\ell = 0$ states: $\text{Err}(\Delta_{T'}) \approx$
 401 10^{-2} and $\text{Err}(\Delta_C) \approx 3 \times 10^{-3}$, meaning that $\text{Err}(\Delta_{T'})/\Delta_{T'} \approx 10^{-3}$ and $\text{Err}(\Delta_C)/\Delta_C \approx 5 \times 10^{-4}$.
 402 Within our precision, we observe very good agreement with the results of [20] (especially for T').

403 Furthermore, the unresummed epsilon expansion is again in agreement with the bootstrap results
 404 for $d \rightarrow 4$. Overall, the picture is consistent with the $\ell = 0$ case discussed earlier¹¹.

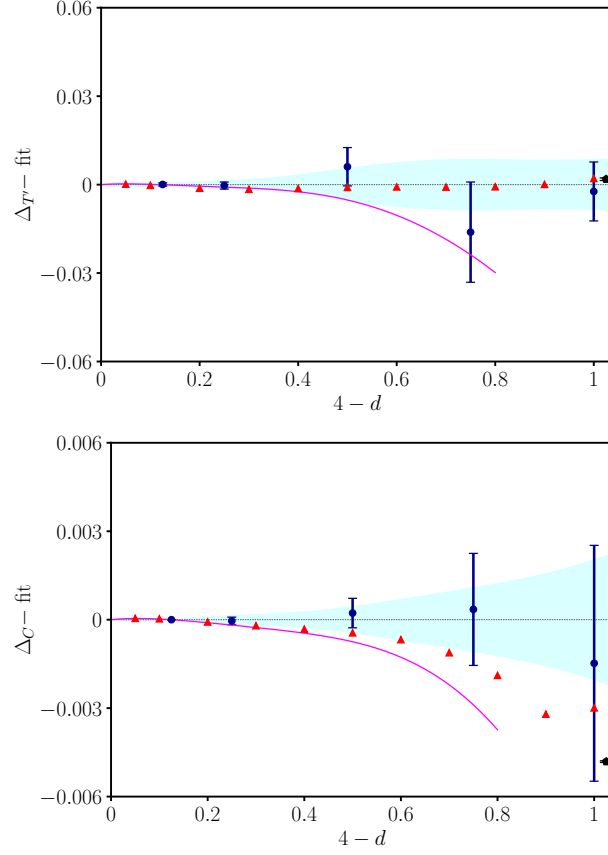


Figure 18: Comparison of scaling dimensions minus best fit for T', C fields: bootstrap (blue round points), navigator method [20] (triangle red points), 3-correlator bootstrap at $d = 3$ [46] (black pentagon) and unresummed epsilon expansion [26, 31, 57, 58] (magenta solid line).

405 The corresponding structure constants are given by the polynomial fits

$$\begin{aligned}
 f_{\sigma\sigma T'}(y) = & 0.026278214y - 0.012019512y^2 - 0.016779681y^3 \\
 & + 0.025762223y^4 - 0.018571573y^5 + 0.006902659y^6 \\
 & - 0.001000504y^7, \quad (\text{conformal bootstrap}), \quad (29)
 \end{aligned}$$

$$\begin{aligned}
 f_{\sigma\sigma C}(y) = & 0.16903085 - 0.122480930y + 0.077087613y^2 - 0.591032947y^3 \\
 & + 1.331591787y^4 - 1.231373513y^5 + 0.512308476y^6 \\
 & - 0.079520247y^7, \quad (\text{conformal bootstrap}). \quad (30)
 \end{aligned}$$

406 They can be compared to the available epsilon expansions [26, 31, 57–59]:

$$f_{\sigma\sigma T'}(y) = 0.02635231y - 0.013176155y^2, \quad (\text{epsilon expansion}), \quad (31)$$

$$\begin{aligned}
 f_{\sigma\sigma C}(y) = & 0.16903085 - 0.12244675y + 0.02131741y^2 \\
 & + 0.002168567y^3 - 0.0019760553y^4, \quad (\text{epsilon expansion}). \quad (32)
 \end{aligned}$$

¹¹The good behavior of the perturbative expansion for larger values of $y \approx 0.8$ is not stressed, since it may be an artifact of the low order of the series.

407 The comparison is shown in Fig. 19. Also in this case we observe good agreement between the
 408 conformal bootstrap polynomials and the epsilon expansion series up to $O(y^3)$ terms.

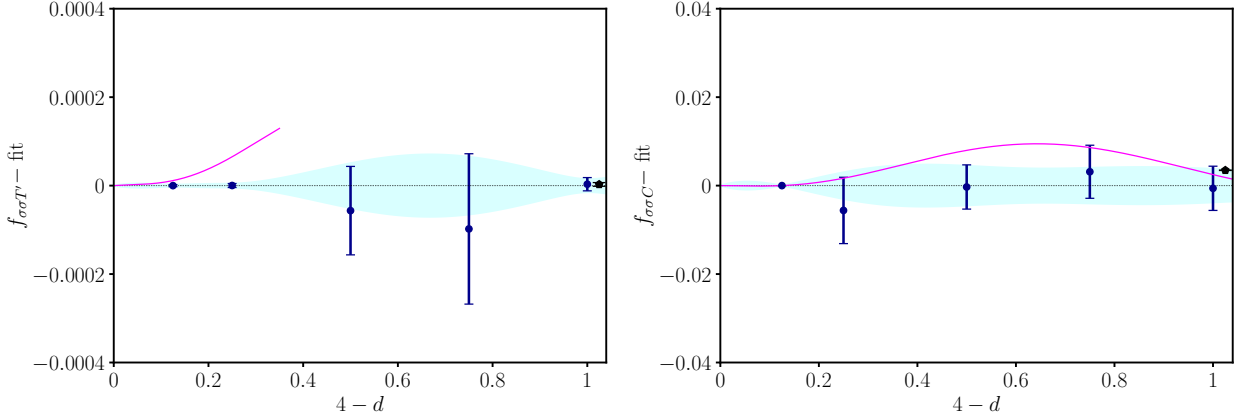


Figure 19: Behavior of structure constants $f_{\sigma\sigma T'}$ and $f_{\sigma\sigma C}$ (round blue points) compared with 3-correlator bootstrap at $d = 3$ [46] (black pentagon) and epsilon expansion (magenta solid line) [57, 58].

409 4.3 Subleading fields ϵ'' and C'

410 The numerical 1-correlator bootstrap approach used in this paper is known to have a limited
 411 precision for states higher up in the conformal spectrum, in particular for our approximation to 190
 412 components of the truncated bootstrap equations. In this section, we show that our identification
 413 of ϵ'' ($\ell = 0$) and C' ($\ell = 4$) has some problems, especially for $d \rightarrow 4$. We explain these difficulties
 414 by using the epsilon expansion for conformal dimensions and structure constants, as well as the
 415 3-correlator bootstrap data [20] in varying dimensions. We think that these aspects are worth
 416 discussing, especially because the $y = 4 - d$ dependence plays a crucial role.

417 We start our analysis from the subleading twist $\ell = 4$ operator C' , for which we find the following
 418 best fit polynomial:

$$\begin{aligned} \Delta_{C'}(y) = & 8 - 0.827053961y - 0.055211344y^2 + 0.053430207y^3 \\ & + 0.010354264y^4 - 0.003205703y^5, \quad (\text{conformal bootstrap}). \end{aligned} \quad (33)$$

419 These data are shown in Fig. 20 (left part). It turns out that C' is degenerate at $d = 4$ with another
 420 field with same dimension and spin, called C'_2 . Their dimensions are known to leading order in the
 421 epsilon expansion,

$$\Delta_{C'}(y) = 8 - 1.555556y, \quad (34)$$

$$\Delta_{C'_2}(y) = 8 - 0.833333y, \quad (\text{epsilon expansion}), \quad (35)$$

422 and are plotted in Fig. 20 with magenta dashed and solid lines, respectively. Near these lines, the
 423 navigator bootstrap results [20] are plotted with gold and red triangles.

424 One sees that our results start at $d \rightarrow 4$ very close to C'_2 (see first coefficient in polynomials (33)
 425 and (34)) and end up near C' at $d = 3$. Therefore, the state we found is a mixture of C' and C'_2 :
 426 better numerical precision would be needed for disentangling the two states near $d \rightarrow 4$, obtained,
 427 e.g., by increasing the number of components approximating the bootstrap equations.

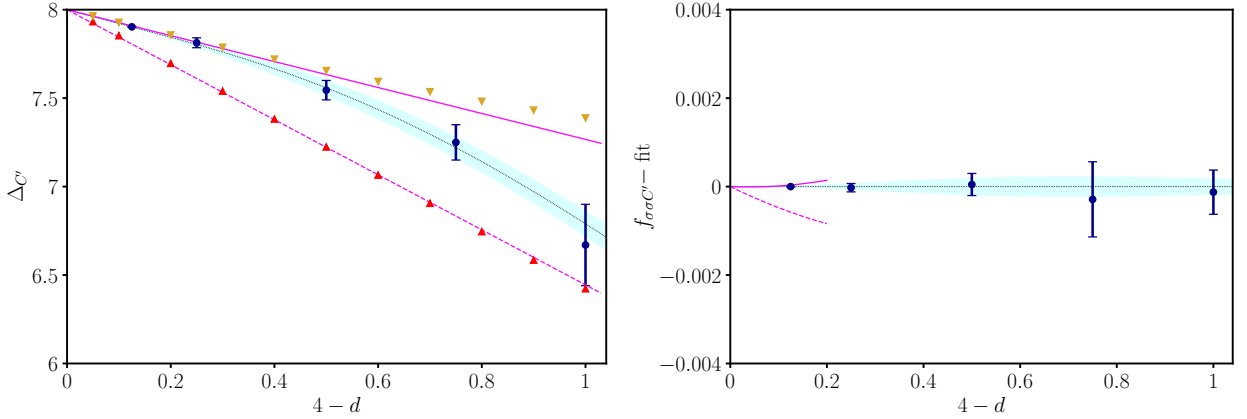


Figure 20: *Scaling dimension and structure constant of would-be C' operator in our bootstrap spectrum (blue circles). Upward red and downward gold triangles represent navigator results for C' and C'_2 [20]. The dashed and solid magenta lines are the corresponding leading-order epsilon expansion.*

428 The fit of the structure constant is given by

$$f_{\sigma\sigma C'}(y) = 0.006871047y - 0.005215834y^2 - 0.003223129y^3 + 0.005087571y^4 - 0.001393464y^5, \quad (\text{conformal bootstrap}), \quad (36)$$

429 and plotted in the right part of Fig. 20. The epsilon-expansion results for C' and C'_2 read,

$$f_{\sigma\sigma C'}(y) = 0.001543806y, \quad (37)$$

$$f_{\sigma\sigma C'_2}(y) = 0.006458202y, \quad (\text{epsilon expansion}), \quad (38)$$

430 and are shown as magenta dashed and solid lines on the right of Fig. 20.

431 These perturbative data show a remarkable fact: for $d < 4$ the state of higher dimension C'_2
 432 has a larger structure constant, contrary to the standard behavior of $f_{\sigma\sigma\mathcal{O}}$ decreasing fast with
 433 $\Delta_{\mathcal{O}}$. It is thus clear that, close to $d = 4$, C'_2 gives the dominant contribution to a putative mixed
 434 $C'-C'_2$ state. This suggests the reason why our results with limited precision start close to C'_2 . The
 435 analysis is confirmed by the bootstrap result for the structure constant in (36): for $d \rightarrow 4$ it fits the
 436 perturbative behavior of $f_{\sigma\sigma C'_2}$, as seen in the right plot of Fig. 20. In conclusion, our subleading
 437 $\ell = 4$ state is identified as C'_2 for $d \rightarrow 4$, but gradually approaches C' in $d = 3$.

438 Another problematic identification concerns the ϵ'' field (corresponding to ϕ^6 in the ϕ^4 theory).
 439 The best fit of bootstrap data gives

$$\Delta_{\epsilon''}(y) = 2.313321845y - 1.678645012y^2 + 0.336440006y^3 + 0.090959178y^4, \quad (\text{conformal bootstrap}), \quad (39)$$

440 while the leading epsilon-expansion result reads [23, 24, 59]:

$$\Delta_{\epsilon''}(y) = 2y - 4.759259y^2, \quad (\text{epsilon expansion}). \quad (40)$$

441 For the structure constant we find

$$f_{\sigma\sigma\epsilon''}(y) = 0.002851280y^2 - 0.003188068y^3 + 0.001218496y^4 - 0.000161879y^5, \quad (\text{conformal bootstrap}); \quad (41)$$

$$f_{\sigma\sigma\epsilon''}(y) = 0.006901444y^2, \quad (\text{epsilon expansion}). \quad (42)$$

442 It is apparent that our bootstrap results do not match the leading perturbative expansion for $d \rightarrow 4$.
 443 The corresponding plots are shown in Fig. 21, where the disagreement with bootstrap results from
 444 Ref. [20] (red triangles) is also seen.

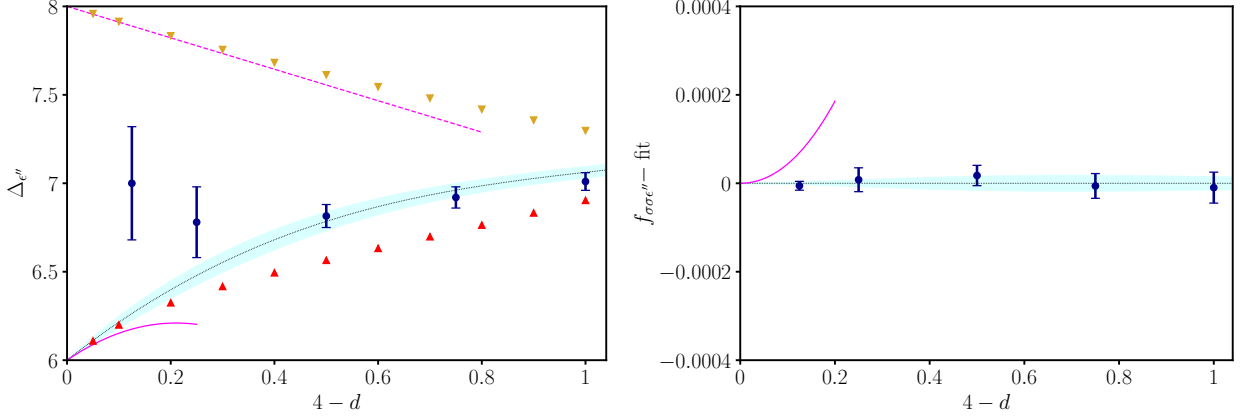


Figure 21: Scaling dimension and structure constant of the would-be ϵ'' operator in our bootstrap spectrum (blue circles). Upward red and downward gold triangles represent navigator results for ϵ'' and ϵ''' [20]. The solid and dashed magenta lines are the corresponding leading-order epsilon expansion, which agree with the navigator results, but not ours.

445 Let us investigate the possibility of another mixing of states near $d \rightarrow 4$. In this case there is no
 446 degenerate field with ϵ'' at $d = 4$. However, the next subleading one $\epsilon''' \sim \square^2 \phi^4$ in the ϕ^4 theory
 447 is present at higher dimension $\Delta_{\epsilon'''} \leq 8$. The epsilon expansion and navigator results for this field
 448 are also shown in Fig. 21 (left part, gold downward triangles). We remark that a mixing of ϵ'' and
 449 ϵ''' was shown to take place at $d = 2.8$, i.e., rather far from $d = 4$ [20].

450 We suppose that the limited resolution of our data finds a state which is a mixture of ϵ'' and ϵ'''
 451 also for $d \rightarrow 4$, but we cannot be certain of this. As for C' and C'_2 , support for this argument could
 452 come from a comparison of the corresponding structure constants $f_{\sigma\sigma\epsilon''}$ and $f_{\sigma\sigma\epsilon'''}$. Unfortunately,
 453 the epsilon expansion of the latter is not available, so we cannot get a definite explanation of our
 454 $\Delta_{\epsilon''}$ data.

455 5 Conclusions

456 In this paper we obtained the conformal dimensions and structure constants of the critical Ising
 457 CFT as a function of varying dimension $4 > d \geq 3$ by using the numerical conformal bootstrap
 458 approach.

459 Our main result is the precise determination of the anomalous dimensions of the $\sigma, \epsilon, \epsilon'$ fields,
 460 which are related to the Ising critical exponents η, ν, ω . Our relatively simple 1-correlator bootstrap
 461 setup is able to compute the d -dependence of these quantities with up to one-per-thousand relative
 462 accuracy; therefore, our findings can be used as a benchmark for future studies in non-integer space
 463 dimension.

464 We presented a detailed comparison of available predictions from different methods. For $d \rightarrow 4$,
 465 our results agree with those from unresummed perturbation theory. This shows two things: that

466 non-perturbative differences, which might effect the bootstrap program or the resummed series,
 467 are negligible for $d \rightarrow 4$. The other non-trivial result is that both approaches agree on the same
 468 analytic continuation in dimension. A possible explanation of this correspondence is provided by
 469 the analytical bootstrap, which on one hand reproduces the epsilon expansion, and on the other
 470 hand uses the same ingredients as the numerical bootstrap.

471 For $3 \leq d < 4$, but away from $d = 4$, the bootstrap data agree very well with other results,
 472 obtained by resummation techniques of the perturbative series, Monte Carlo simulations, and other
 473 bootstrap approaches. In the whole $4 > d \geq 3$ range we find overall consistency among the different
 474 approaches; improvements are needed by adding further terms to the perturbative series in $d = 3$,
 475 as the current state of the art still shows a $O(10^{-3})$, $O(10^{-2})$ discrepancy, respectively for ν and
 476 ω , and in general much larger error bars than bootstrap and Monte Carlo results.

477 In addition, we obtained results for the conformal dimensions of higher-order fields and structure
 478 constants. As for the former, we are able to precisely compute bootstrap data related to the lowest-
 479 lying spinful fields T' ($\ell = 2$) and C ($\ell = 4$) with comparable precision to that for $\ell = 0$. We find
 480 that both the central charge, and the OPE coefficients of low-lying fields are obtained with higher
 481 precision than the corresponding anomalous dimensions. The structure constants agree well with
 482 other bootstrap findings in the $d \rightarrow 3$ regime and with perturbation theory close to $d = 4$, confirming
 483 the overall picture found for critical exponents.

484 A possible future development is to improve current bootstrap results in the region $3 > d \geq 2$, in
 485 order to better understand how the $d = 3$ theory approaches the $d = 2$ Virasoro minimal model. To
 486 this aim, it is important to go beyond the lowest-lying states and precisely probe higher-dimensional
 487 and higher-spin fields. Improved 3-correlator bootstrap protocols, such as the recently proposed
 488 navigator method, may be well suited here.

489 Acknowledgements

490 We are grateful to C. Bonati, R. Guida, J. Henriksson, S. Kousvos, L. Maffi, R. Pisarski,
 491 M. Reehorst, S. Rychkov, M. Serone and B. Sirois for useful discussions. CB acknowledges the
 492 support of the Italian Ministry of Education, University and Research under the project PRIN
 493 2017E44HRF, “Low dimensional quantum systems: theory, experiments and simulations”. Numerical
 494 computations have been performed on the *Zefiro* cluster of the Scientific Computing Center
 495 at INFN Pisa.

496 Appendix

497 A Orthogonal polynomial regression

498 Standard polynomial regression of the data set $S \equiv \{x_i, y_i, \Delta y_i\}_{i=1}^N$ is achieved by minimizing

$$\chi^2 = \sum_{k=1}^N \left(\frac{y_k - f(x_k)}{\Delta y_k} \right)^2, \quad (43)$$

499 with respect to the parameters $\{c_i\}_{i=0}^d$ of the fit function,

$$f_n(x) = \sum_{r=0}^n c_r x^r. \quad (44)$$

500 The degree n of the polynomial is not known a priori.

501 A smarter fit is obtained by changing the basis in which the polynomial is expressed:

$$\mathcal{B}_{\text{naive}} = \{1, x, x^2, \dots, x^d\} \rightarrow \mathcal{B}_{\text{ortho}} = \{P_0(x), P_1(x), P_2(x), \dots, P_d(x)\}, \quad (45)$$

502 where the polynomials $P_k(x)$ (of degree k) are chosen to be *orthogonal* on the independent variables
503 of the dataset S , i.e.:

$$\langle P_r(x) P_s(x) \rangle_S = \frac{1}{N} \sum_{k=1}^N P_r(x_k) P_s(x_k) = k_r^2 \delta_{rs}, \quad (46)$$

504 where k_r are constants. With this choice, the fit function becomes

$$f_n(x) = \sum_{r=0}^n \alpha_r P_r(x). \quad (47)$$

505 The best fit is obtained by minimizing χ^2 in Eq. (43). The advantage of the orthogonal polynomial
506 regression is that the coefficients α_r do not depend on the α_s with $s > r$, i.e., adding higher-degree
507 polynomials $r > n$ to $f_n(x)$ does not change the value of α_r with $r \leq n$ within the statistical
508 errors [48]. Thus, this procedure is better suited to assess the optimal degree of the polynomial.

509 The expression of the polynomials $P_r(x)$ is known in the literature. In this work, we follow the
510 conventions of Ref. [48]. We start by fixing the $r = 0$ and $r = 1$ polynomials as

$$P_0(x) = 1, \quad P_1(x) = 2(x - a_1), \quad a_1 = \frac{1}{N} \sum_{k=1}^N x_k \equiv \bar{x}. \quad (48)$$

511 Higher-order polynomials with $r \geq 2$ are obtained through the recursive relation [48],

$$P_{r+1}(x) = 2(x - a_{r+1})P_r(x) - b_r P_{r-1}(x), \quad (49)$$

512 where the coefficients a_{r+1} and b_r are given by

$$a_{r+1} = \frac{\sum_{k=1}^N x_k P_r^2(x_k)}{\sum_{k=1}^N P_r^2(x_k)}, \quad b_r = \frac{\sum_{k=1}^N P_r^2(x_k)}{\sum_{k=1}^N P_{r-1}^2(x_k)}. \quad (50)$$

513 In this work, we find the best fitting polynomial for $\gamma_{\mathcal{O}}$ and $f_{\sigma\sigma\mathcal{O}}$ as a function of $y = 4 - d$. We
514 always assume their known analytic value for $d = 4$, for example $\gamma_{\mathcal{O}}(d = 4) = 0$. To enforce such
515 constraint, it is sufficient to use as fit function

$$h_n(x) = f_n(x) - f_n(0) = \sum_{r=1}^n \tilde{\alpha}_r [P_r(x) - P_r(0)]. \quad (51)$$

516 Finally, we reconstruct the original expansion in the naive basis by summing all equal monomials
 517 among every $P_r(x)$ included in the fit function:

$$h_n(x) = \sum_{r=1}^n \tilde{\alpha}_r [P_r(x) - P_r(0)] = \sum_{r=1}^n \tilde{c}_r x^r, \quad (52)$$

518 where

$$\tilde{c}_r = \sum_{l=r}^n \tilde{\alpha}_l \left. \frac{d^r P_l(x)}{dx^r} \right|_{x=0}. \quad (53)$$

519 Once the two expansions are properly matched, the coefficients obtained from orthogonal poly-
 520 nomials agree with those obtained using a standard polynomial fit. The advantage of orthogonal
 521 polynomials resides in their improved numerical stability, which results in an improved precision in
 522 the computation of the c_i .

523 Finally, once the best fitting polynomial is obtained, we assign an error to our best fit function
 524 $h_n(x)$ through standard error propagation, via the so-called parameter covariance matrix,

$$C_{ij} \equiv \text{Cov}(\tilde{\alpha}_i, \tilde{\alpha}_j). \quad (54)$$

525 Let us define $v_i(x)$ as the gradient of the fit function with respect to the i^{th} fit parameter,

$$v_i(x) = \frac{\partial h_n(x | \vec{\alpha})}{\partial \tilde{\alpha}_i}. \quad (55)$$

526 The error on the best fitting polynomial is

$$\text{Err}(h_n)(x) = v^T(x) C v(x) = C_{ij} v_i(x) v_j(x). \quad (56)$$

527 The best fit of $\gamma_{\mathcal{O}}(y)$ via orthogonal polynomial regression was done by using the `curve_fit` routine
 528 from the standard Python library `scipy`.

529 B Example of series resummation

530 In this appendix, we discuss the perturbative expansion of a toy model in dimension zero:

$$\mathcal{I}(g) \equiv \int_{-\infty}^{\infty} \frac{dx}{\sqrt{2\pi}} e^{-\frac{x^2}{2} - gx^4}. \quad (57)$$

531 Its perturbative expansion is

$$\mathcal{I}(g) = \sum_{n=0}^{\infty} a_n (-g)^n, \quad a_n = \frac{(4n)!}{2^{2n} (2n)! n!} \underset{n \rightarrow \infty}{\sim} \frac{2^{4n}}{\sqrt{2\pi n}} \times n!. \quad (58)$$

532 The analytic continuation of the integral (57) from $\text{Re}(g) > 0$ to the full complex plane is given by
 533 a second-kind modified Bessel K -function:

$$\mathcal{I}(g) = \frac{1}{4\sqrt{\pi g}} e^{\frac{1}{32g}} K_{\frac{1}{4}} \left(\frac{1}{32g} \right). \quad (59)$$

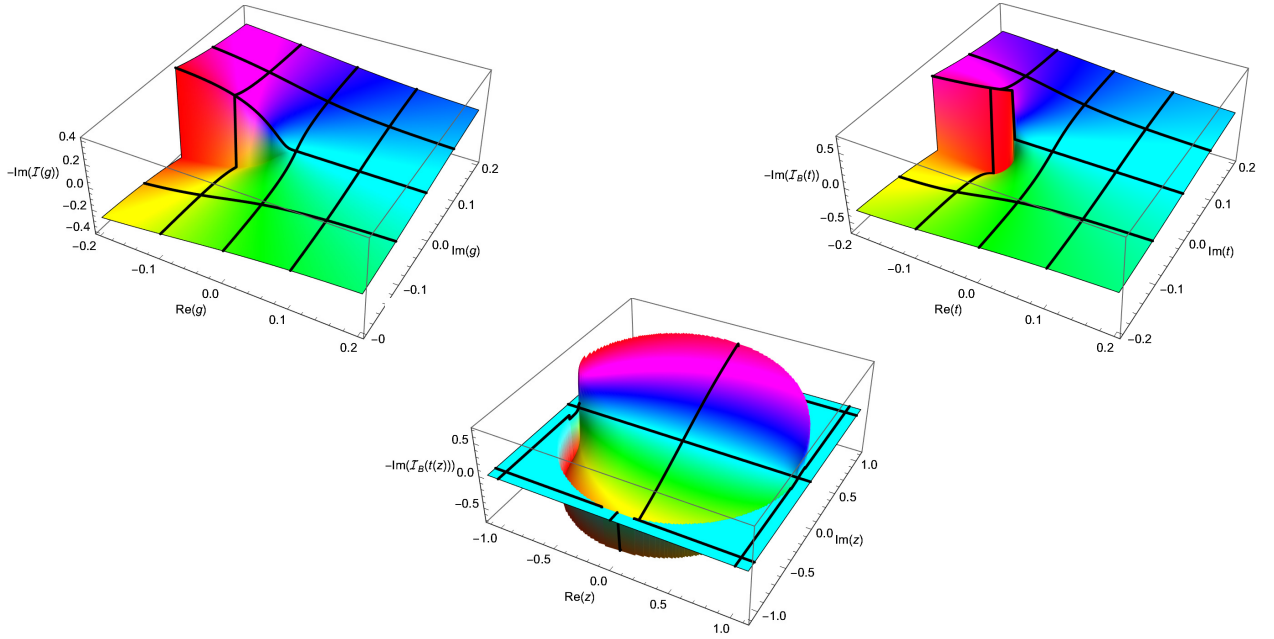


Figure 22: The branch cut in $\mathcal{I}(g)$ (top left) and $\mathcal{I}_B(t)$ (top right). While the former starts at $g = 0$, the latter is moved to $g = -1/16$. The lower plot shows $\mathcal{I}_B(t(z))$, which now has a branch-cut singularity at $|z| = 1$. (We set $\mathcal{I}_B(t(z))$ to 0 outside the disc $|z| \geq 1$.)

534 Using the asymptotic behavior of $K_{\frac{1}{4}}(z)$ for $z \rightarrow \infty$, one sees that the exponential prefactor is
 535 canceled, and the series (58) recovered. Note that $\mathcal{I}(g)$ has a cut on the whole negative real axis,
 536 see Fig. 22.

537 In field theory, the divergent series is analytically continued without the knowledge of its exact
 538 expression. Let us explain the strategy on the example of integral (57). The basic idea [50] to
 539 obtain a convergent series out of Eq. (58), is to divide each term by $n!$, defining the *Borel transform*
 540 $\mathcal{I}_B(t)$ of the series. In a second step, one reconstructs the original series via an integral transform:

$$\mathcal{I}_B(t) \equiv \sum_{n=0}^{\infty} \frac{a_n}{n!} (-t)^n, \quad \mathcal{I}(g) = \int_0^{\infty} dt e^{-t} \mathcal{I}_B(tg). \quad (60)$$

541 In our example we know the analytic expression in terms of the first-kind complete elliptic integral
 542 function

$$\mathcal{I}_B(t) = \frac{2K_{\text{elliptic}}\left(\frac{1}{2} - \frac{1}{2\sqrt{16t+1}}\right)}{\pi \sqrt[4]{16t+1}}. \quad (61)$$

543 The Borel transform $\mathcal{I}_B(t)$ has a finite radius of convergence, denoted by $-t_{\text{bc}}$ (equal to $1/16$ in
 544 our example). As a consequence, the start of the branch cut is moved from $g = 0$ to $t = t_{\text{bc}} < 0$,
 545 see figure 22. Since the radius of convergence of $\mathcal{I}_B(t)$ is still finite, the integral transform (60)
 546 does not work as written. One first has to continue $\mathcal{I}_B(t)$ to the domain $0 \leq t < \infty$. This can be
 547 achieved by replacing the known truncated series via a converging Padé approximant, leading to a
 548 *Padé-Borel resummation*.

549 A more powerful strategy is to use a conformal mapping. The most common ansatz is to assume
 550 that at $t = t_{\text{bc}} < 0$ a cut-singularity starts, which extends on the negative real axis to $t = -\infty$.

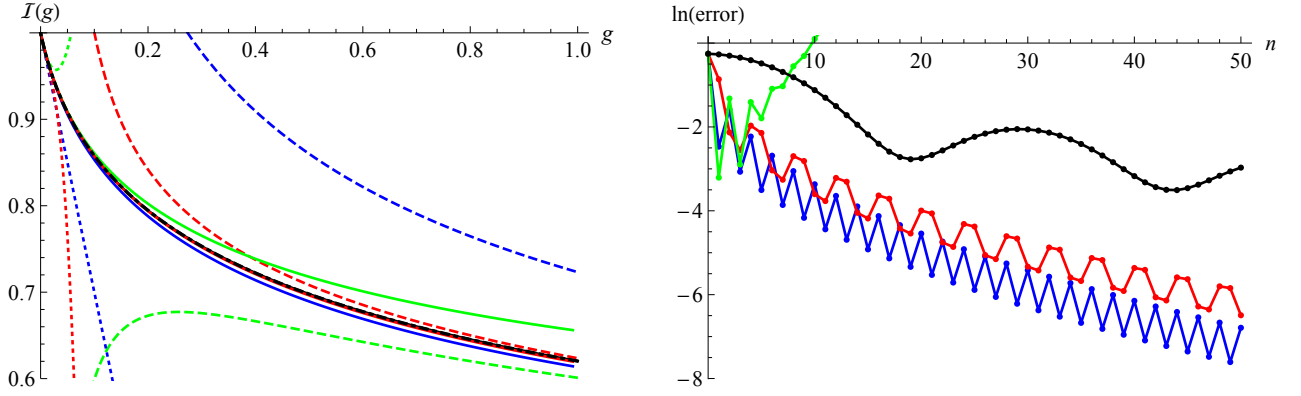


Figure 23: Left: function $\mathcal{I}(g)$ (black, thick, dot-dashed) and its diverse approximations. Dotted for the series expansion at order 1 (blue), 2 (green), and 3 (red). Solid for the resummed series at the same order. Dashed for the large- g expansion (same color code). Right: deviation of the resummed series (65) from the exact result (61) for $g = 10$ as a function of n , assuming one knows t_{bc} only approximately. In blue for $t_{bc} = -1/16$ (the exact result), in red $t_{bc} = -1/32$ (a conservative guess), in black $t_{bc} = -1/1000$ (much too small). Resummation with $t_{bc} = -1/15$ (green) does not work. We see that conform to expectations, taking a too small value for $-t_{bc}$, the series converges more slowly, while taking a too large value of $-t_{bc}$ the series does not converge.

551 One first maps the complex plane with the expected branch cut of $\mathcal{I}_B(t)$ onto the inside of the
 552 unit-circle:

$$z = \frac{\sqrt{1 - t/t_{bc}} - 1}{\sqrt{1 - t/t_{bc}} + 1} \iff t = \frac{-4t_{bc}z}{(z-1)^2}. \quad (62)$$

553 Next one constructs a series in z by expanding both sides in this variable:

$$f(z) \equiv \sum_{n=0}^{\infty} c_n z^n = \sum_{n=0}^{\infty} \frac{a_n (-t(z))^n}{n!} = \mathcal{I}_B(t(z)). \quad (63)$$

554 This series is expected to converge for $|z| < 1$, a fact we can check for our example (but which is
 555 difficult to prove in general):

$$f(z) = 1 - \frac{3z}{4} + \frac{9z^2}{64} - \frac{51z^3}{256} + \frac{1353z^4}{16384} - \frac{7347z^5}{65536} + \frac{61617z^6}{1048576} + \mathcal{O}(z^7). \quad (64)$$

556 Given n terms in the original series, we know $f(z)$ up to the same order. Using this approximation
 557 for $f(z)$, we finally obtain:

$$\mathcal{I}(g) = \int_0^{\infty} dt e^{-t} \mathcal{I}_B(tg) = \frac{1}{g} \int_0^{\infty} dt e^{-t/g} \mathcal{I}_B(t) = \frac{1}{g} \int_0^1 dz t'(z) e^{-t(z)/g} f(z). \quad (65)$$

558 The result of this resummation is shown on Fig. 23. First, in black is the analytic result (59). Next
 559 are the first three orders in several expansions, using the same color code for order 1 (blue), 2 (green),
 560 and 3 (red): first the direct expansion in g (dotted), then in solid the resummed expansion (65).
 561 Dashed, we show a large- g expansion obtained by changing variables $gx^4 \rightarrow y$ in the integral (57),

562 and then expanding the integrand in powers of $1/\sqrt{g}$:

$$\begin{aligned} \mathcal{I}(g) &= \frac{1}{2\sqrt{2\pi}\sqrt[4]{g}} \int_0^\infty dy \frac{e^{-\frac{\sqrt{y}}{2\sqrt{g}}-y}}{y^{\frac{3}{4}}} \\ &= \frac{1}{2\sqrt{2\pi}\sqrt[4]{g}} \left[\Gamma\left(\frac{1}{4}\right) - \frac{2}{3} \frac{\Gamma\left(\frac{7}{4}\right)}{\sqrt{g}} + \frac{\Gamma\left(\frac{5}{4}\right)}{8g} + \mathcal{O}\left(g^{-\frac{5}{4}}\right) \right]. \end{aligned} \quad (66)$$

563 References

- 564 [1] K. G. Wilson and M. E. Fisher, “*Critical exponents in 3.99 dimensions*”, Phys. Rev. Lett. **28**
565 (1972) 240.
- 566 [2] J. C. Le Guillou and J. Zinn-Justin, “*Accurate critical exponents for Ising like systems in*
567 *noninteger dimensions*”, J. Phys. (Les Ulis) **48** (1987) 19.
- 568 [3] R. Guida and J. Zinn-Justin, “*Critical exponents of the N -vector model*”, J. Phys. A **31** (1998)
569 8103.
- 570 [4] A. Pelissetto and E. Vicari, “*Critical phenomena and renormalization group theory*”, Phys.
571 Rept. **368** (2002) 549.
- 572 [5] V. V. Prudnikov, P. V. Prudnikov and A. A. Fedorenko, “*Field-theory approach to critical*
573 *behavior of systems with long-range correlated defects*”, Phys. Rev. B **62** (2000) 8777.
- 574 [6] C. Behan, L. Rastelli, S. Rychkov and B. Zan, “*A scaling theory for the long-range to short-*
575 *range crossover and an infrared duality*”, J. Phys. A **50** (2017) 354002.
- 576 [7] N. Defenu, A. Trombettoni and S. Ruffo, “*Criticality and Phase Diagram of Quantum Long-*
577 *Range $O(N)$ models*”, Phys. Rev. B **96** (2017) 104432.
- 578 [8] A. W. W. Ludwig, “*Critical behavior of the two-dimensional random q -state Potts model by*
579 *expansion in $(q - 2)$* ”, Nucl. Phys. B **285** (1987) 97–142.
- 580 [9] J. L. Jacobsen, P. Le Doussal, M. Picco, R. Santachiara and K. J. Wiese, “*Critical interfaces*
581 *in the random-bond Potts model*”, Phys. Rev. Lett. **102** (2009) 070601.
- 582 [10] Z. Komargodski and D. Simmons-Duffin, “*The Random-Bond Ising Model in 2.01 and 3 Di-*
583 *mensions*”, J. Phys. A **50** (2017) 154001.
- 584 [11] G. Parisi and N. Sourlas, “*Random magnetic fields, supersymmetry, and negative dimensions*”,
585 Phys. Rev. Lett. **43** (1979) 744.
- 586 [12] A. Kaviraj, S. Rychkov and E. Trevisani, “*Parisi–Sourlas Supersymmetry in Random Field*
587 *Models*”, Phys. Rev. Lett. **129** (2022) 045701.
- 588 [13] K. J. Wiese, “*Theory and experiments for disordered elastic manifolds, depinning, avalanches,*
589 *and sandpiles*”, Rep. Prog. Phys. **85** (2022) 086502.
- 590 [14] R. Rattazzi, V. S. Rychkov, E. Tonni and A. Vichi, “*Bounding scalar operator dimensions in*
591 *4D CFT*”, JHEP **0812** (2008) 031.

- 592 [15] S. El-Showk, M. F. Paulos, D. Poland, S. Rychkov, D. Simmons-Duffin and A. Vichi, “*Solving the 3d Ising Model with the Conformal Bootstrap II. c -Minimization and Precise Critical*
593 *Exponents*”, J. Stat. Phys. **157** (2014) 869.
594
- 595 [16] D. Poland, S. Rychkov and A. Vichi, “*The Conformal Bootstrap: Theory, Numerical Tech-*
596 *niques, and Applications*”, Rev. Mod. Phys. **91** (2019) 015002.
- 597 [17] S. El-Showk, M. Paulos, D. Poland, S. Rychkov, D. Simmons-Duffin and A. Vichi, “*Conformal*
598 *Field Theories in Fractional Dimensions*”, Phys. Rev. Lett. **112** (2014) 141601.
- 599 [18] B. Sirois, “*Navigating through the $O(N)$ archipelago*”, [arXiv:2203.11597 [hep-th]].
- 600 [19] A. Cappelli, L. Maffi and S. Okuda, “*Critical Ising Model in Varying Dimension by Conformal*
601 *Bootstrap*”, JHEP **01** (2019) 161.
- 602 [20] J. Henriksson, S. R. Kousvos, M. Reehorst, “*Spectrum continuity and level repulsion: the*
603 *Ising CFT from infinitesimal to finite ϵ* ”, [arXiv:2207.10118 [hep-th]].
- 604 [21] A. A. Belavin, A. M. Polyakov and A. B. Zamolodchikov, “*Infinite Conformal Symmetry in*
605 *Two-Dimensional Quantum Field Theory*”, Nucl. Phys. B **241** (1984) 333.
- 606 [22] P. Di Francesco, P. Mathieu and D. Senechal, “*Conformal Field Theory*”, Springer-Verlag,
607 New York (1997).
- 608 [23] S. Rychkov and Z. M. Tan, “*The ϵ -expansion from conformal field theory*”, J. Phys. A **48**
609 (2015) 29FT01.
- 610 [24] F. Gliozzi, A. L. Guerrieri, A. C. Petkou and C. Wen, “*The analytic structure of conformal*
611 *blocks and the generalized Wilson–Fisher fixed points*”, JHEP **1704** (2017) 056.
- 612 [25] L. F. Alday, “*Large Spin Perturbation Theory for Conformal Field Theories*”, Phys. Rev. Lett.
613 **119** (2017) 111601.
- 614 [26] L. F. Alday, J. Henriksson and M. van Loon, “*Taming the ϵ -expansion with large spin pertur-*
615 *bation theory*”, JHEP **1807** (2018) 131.
- 616 [27] A. Bissi, A. Sinha and X. Zhou, “*Selected Topics in Analytic Conformal Bootstrap: A Guided*
617 *Journey*”, [arXiv:2202.08475 [hep-th]].
- 618 [28] T. Hartman, D. Mazac, D. Simmons-Duffin and A. Zhiboedov, “*Snowmass White Paper: The*
619 *Analytic Conformal Bootstrap*”, [arXiv:2202.11012 [hep-th]].
- 620 [29] F. Bertucci, J. Henriksson and B. McPeak, “*Analytic bootstrap of mixed correlators in the*
621 *$O(n)$ CFT*”, [arXiv:2205.09132 [hep-th]].
- 622 [30] J. Henriksson, “*The critical $O(N)$ CFT: Methods and conformal data*”, [arXiv:2201.09520
623 [hep-th]].
- 624 [31] J. Henriksson and M. Van Loon, “*Critical $O(N)$ model to order ϵ^4 from analytic bootstrap*”,
625 J. Phys. A **52** (2019) 025401.
- 626 [32] M. Hogervorst, S. Rychkov and B. C. van Rees, “*Unitarity violation at the Wilson–Fisher fixed*
627 *point in $4 - \epsilon$ dimensions*”, Phys. Rev. D **93** (2016) 125025.

- 628 [33] D. Simmons-Duffin, “A *Semidefinite Program Solver for the Conformal Bootstrap*”, JHEP
629 **1506** (2015) 174.
- 630 [34] S. El-Showk and M. F. Paulos, “*Bootstrapping Conformal Field Theories with the Extremal*
631 *Functional Method*”, Phys. Rev. Lett. **111** (2013) 241601.
- 632 [35] S. El-Showk and M. F. Paulos, “*Extremal bootstrapping: go with the flow*”, JHEP **1803** (2018)
633 148.
- 634 [36] M. Kompaniets, “*Prediction of the higher-order terms based on Borel resummation with con-*
635 *formal mapping*”, J. Phys. Conf. Ser. **762** (2016) 012075.
- 636 [37] D. V. Batkovich, K. G. Chetyrkin and M. V. Kompaniets, “*Six loop analytical calculation of*
637 *the field anomalous dimension and the critical exponent η in $O(n)$ -symmetric ϕ^4 model*”, Nucl.
638 Phys. B **906** (2016) 147.
- 639 [38] M. V. Kompaniets and E. Panzer, “*Minimally subtracted six loop renormalization of $O(n)$ -*
640 *symmetric ϕ^4 theory and critical exponents*”, Phys. Rev. D **96** (2017) 036016.
- 641 [39] M. V. Kompaniets and K. J. Wiese, “*Fractal dimension of critical curves in the $O(n)$ -*
642 *symmetric ϕ^4 model and crossover exponent at 6-loop order: Loop-erased random walks, self-*
643 *avoiding walks, Ising, XY, and Heisenberg models*”, Phys. Rev. E **101** (2020) 012104.
- 644 [40] M. Hasenbusch, “*Finite size scaling study of lattice models in the three-dimensional Ising*
645 *universality class*”, Phys. Rev. B **82** (2010) 174433.
- 646 [41] A. M. Ferrenberg, J. Xu and D. P. Landau, “*Pushing the limits of monte carlo simulations for*
647 *the three-dimensional Ising model*”, Phys. Rev. E **97** (2018) 043301.
- 648 [42] M. Hasenbusch, “*Restoring isotropy in a three-dimensional lattice model: The Ising universal-*
649 *ity class*”, Phys. Rev. B **104** (2021) 014426.
- 650 [43] I. Balog, H. Chaté, B. Delamotte, M. Marohnic and N. Wschebor, “*Convergence of Nonpertur-*
651 *bative Approximations to the Renormalization Group*”, Phys. Rev. Lett. **123** (2019) 240604.
- 652 [44] N. Dupuis, L. Canet, A. Eichhorn, W. Metzner, J.M. Pawłowski, M. Tissier and N. Wschebor,
653 “*The nonperturbative functional renormalization group and its applications*”, Phys. Rep. **910**
654 (2021) 1.
- 655 [45] F. Kos, D. Poland and D. Simmons-Duffin, “*Bootstrapping Mixed Correlators in the 3D Ising*
656 *Model*”, JHEP **1411** (2014) 109.
- 657 [46] D. Simmons-Duffin, “*The Lightcone Bootstrap and the Spectrum of the 3d Ising CFT*”, JHEP
658 **1703** (2017) 086.
- 659 [47] M. Reehorst, S. Rychkov, D. Simmons-Duffin, B. Sirois, N. Su and B. van Rees, “*Navigator*
660 *Function for the Conformal Bootstrap*”, SciPost Phys. **11** (2021) 072.
- 661 [48] G. A. F. Seber and A. J. Lee, “*Linear Regression Analysis*” (Second ed.), John Wiley & Sons,
662 Inc., Hoboken, New Jersey (2003).
- 663 [49] M. Reehorst, “*Rigorous bounds on irrelevant operators in the 3d Ising model CFT*”, JHEP **09**
664 (2022) 177.

- 665 [50] J. Zinn-Justin, “*Quantum Field Theory and Critical Phenomena*” (Fourth ed.), Clarendon
666 Press, Oxford (2002).
- 667 [51] A. N. Vasiliev, “*The field theoretic renormalization group in critical behavior theory and*
668 *stochastic dynamics*”, Chapman & Hall/CRC, Boca Raton (2004).
- 669 [52] O. Schnetz, “*Numbers and Functions in Quantum Field Theory*”, Phys. Rev. D **97** (2018)
670 085018.
- 671 [53] G. V. Dunne and M. Meynig, “*Instantons or renormalons? Remarks on $\phi_{d=4}^4$ theory in the*
672 *MS scheme*”, Phys. Rev. D **105** (2022) 025019.
- 673 [54] I. Aniceto, G. Basar and R. Schiappa, “*A Primer on Resurgent Transseries and Their Asymp-*
674 *totics*”, Phys. Rept. **809** (2019) 1.
- 675 [55] H. Mera, T. G. Pedersen and B. K. Nikolić, “*Fast summation of divergent series and resurgent*
676 *transseries from Meijer-G approximants*”, Phys. Rev. D **97** (2018) 105027.
- 677 [56] G. Sberveglieri, M. Serone and G. Spada, “*Renormalization scheme dependence, RG flow, and*
678 *Borel summability in ϕ^4 Theories in $d < 4$* ”, Phys. Rev. D **100** (2019) 045008.
- 679 [57] R. Gopakumar, A. Kaviraj, K. Sen and A. Sinha, “*Conformal Bootstrap in Mellin Space*”,
680 Phys. Rev. Lett. **118** (2017) 081601.
- 681 [58] R. Gopakumar, A. Kaviraj, K. Sen and A. Sinha, “*A Mellin space approach to the conformal*
682 *bootstrap*”, JHEP **1705** (2017) 027.
- 683 [59] S. E. Derkachov and A. N. Manashov, “*On the stability problem in the $O(N)$ nonlinear sigma*
684 *model*”, Phys. Rev. Lett. **79** (1997) 1423.